Cavitation in Pharmaceutical Manufacturing and Shipping

Donn Sederstrom
University of Denver

Cavitation in Pharmaceutical Manufacturing and Shipping

Abstract

Therapeutic proteins are used to successfully treat hemophilia, Crohn's Disease, diabetes, and cancer. Recent product recalls have occurred because of sub-visible particle formation resulting from the inherent instability of proteins. It has been suggested that particle formation is associated with late stage processing steps of filling, shipping, and delivery. Previous work at the University of Denver demonstrated that fluid cavitation can generate a large number of sub-visible protein particles in ultra clean formulations, but that mitigation can be achieved with fluid property manipulation. The goal of this research was to (1) assess the risk of cavitation under common pharmaceutical manufacturing conditions (i.e., pipe contraction and pumps), (2) establish a simple threshold criterion, and (3) suggest a series of mitigation techniques based on these thresholds. To accomplish these tasks, computational fluid dynamic simulations for a variety of pipe contraction and vial drop conditions were performed. The impact of geometry, fluid properties and operating conditions were varied to establish thresholds and mitigation strategies. The results of this research show that reducing the turbulence in a fluid system will cause the fluid to be less likely to cavitate. Additionally, threshold bounds were created that establish a definitive transition at which cavitation will occur.

Document Type

Thesis

Degree Name

M.S.

Department

Mechanical Engineering

First Advisor

Corinne S. Lengsfeld, Ph.D.

Second Advisor

Peter Laz

Third Advisor

Breigh Roszelle

Keywords

Cavitation, Computation fluid dynamics, CFD, Critical pressure, Fluid solid interaction, FSI, Pharmaceutical, Proteins

Subject Categories

Biomechanical Engineering | Engineering | Mechanical Engineering

Publication Statement

CAVITATION IN PHARMACEUTICAL MANUFACTURING AND SHIPPING

_____

A Thesis

Presented to

the Faculty of Engineering and Computer Science

University of Denver

_____

In Partial Fulfillment

of the Requirements for the Degree

Master of Science

_____

by

Donn R. Sederstrom

March 2013

Advisor: Corinne S. Lengsfeld

Author: Donn R. Sederstrom
Title: CAVITATION IN PHARMACEUTICAL MANUFACTURING AND SHIPPING
Advisor: Corinne S. Lengsfeld
Degree Date: March 2013

Abstract

Therapeutic proteins are used to successfully treat hemophilia, Crohn's Disease, diabetes, and cancer. Recent product recalls have occurred because of sub-visible particle formation resulting from the inherent instability of proteins. It has been suggested that particle formation is associated with late stage processing steps of filling, shipping, and delivery. Previous work at the University of Denver demonstrated that fluid cavitation can generate a large number of sub-visible protein particles in ultra clean formulations, but that mitigation can be achieved with fluid property manipulation. The goal of this research was to (1) assess the risk of cavitation under common pharmaceutical manufacturing conditions (i.e., pipe contraction and pumps), (2) establish a simple threshold criterion, and (3) suggest a series of mitigation techniques based on these thresholds. To accomplish these tasks, computational fluid dynamic simulations for a variety of pipe contraction and vial drop conditions were performed. The impact of geometry, fluid properties and operating conditions were varied to establish thresholds and mitigation strategies. The results of this research show that reducing the turbulence in a fluid system will cause the fluid to be less likely to cavitate. Additionally, threshold bounds were created that establish a definitive transition at which cavitation will occur.

Acknowledgements

The author wishes to thank Dr. Corinne Lengsfeld for her continued support and the entire lab group for creating a joyful and entertaining work environment. Additionally, the author want to thank his parents, brothers, and extended family for always providing me encouragement and support through my many years of school.

Table of Contents

List of Figures

List of Tables

Nomenclature

A	Experimental constant
a	Acceleration, m/s^2
B	Experimental constant
C	Experimental constant
C_1	Experimental constant
C_2	Experimental constant
Ca	Cavitation number
C_{con}	Solution concentration, mg/mL
C_p	Pressure recovery coefficient
c	Speed of sound, m/s
D_{major}	Inlet diameter, m
D_{minor}	Outlet diameter, m
D_r	Diameter ratio
E	Total fluid energy, J
E_v	Isentropic bulk modulus, N/m^2
$\vec{F}$	External body forces in each direction, N
$\vec{g}$	Gravitational acceleration, m/s^2
h	Enthalpy, J/kg
h_s	Thickness of the solid, m
$\vec{j}$	Diffusion flux, s^{-1}
k	Turbulent kinetic energy, m^2/s^2

k_{eff}	Effective thermal conductivity of the fluid, W/m-K
L	Characteristic length or length of the fluid passageway, m
m	Mass in the system, kg
$\dot{m}$	Mass flow rate, kg/m^3
$\dot{m}_{pq}$	Mass transfer from phase p to q, kg/s
$\dot{m}_{qp}$	Mass transfer from phase q to p, kg/s
P_c	Critical pressure, Pa
P_{in}	Inlet pressure, Pa
P_{local}	Local low pressure, Pa
P_{out}	Outlet pressure, Pa
P_{vap}	Vapor pressure, Pa
p	Pressure, Pa
R	Radius of the fluid passageway, m
Re	Reynolds number
S_h	Volumetric energy source, W/m^3
S_m	Mass source term, kg/s
T	Bulk fluid temperature, K
z	Height, m
t	Time, s
v	Velocity magnitude, m/s
$\vec{v}$	Velocity vector, m/s
α_q	Volume fraction for phase q

γ	Kinematic viscosity, m^2/s
ε	Energy dissipation rate, J/s
η	Kolmogorov length scale, m
μ	Viscosity, kg/m-s
ρ	Density, kg/m^3
ρ_f	Density of the fluid, kg/m^3
ρ_s	Density of the solid, kg/m^3
ρ_q	Density of the fluid q, kg/m^3
∇	Derivative in 3 dimensional space
$\bar{\bar{\tau}}$	Stress tensor, Pa
$\bar{\bar{\tau}}_{eff}$	Effective stress tensor, Pa

Chapter One: Motivation

<u>Introduction</u>

Therapeutic proteins are used to treat hemophilia, Crohn's Disease, diabetes, and cancer [1]. These proteins are inherently unstable which can cause them to denature and aggregate [1–5]. If the patient is to receive the designed effect of the therapeutic protein, the protein must be delivered in the design structure and shape, known as the native state. Studies have shown that there can be adverse effects if proteins are not in their native state. These adverse effects can include reduction in responsiveness to the drug therapy eventually leading to immunogenicity [3–5]. Studies have also shown that therapeutic proteins are highly susceptible to degradation because of their weak bonding structures [2]. The use of therapeutic proteins is on the rise as they are becoming more affordable and the availability of drugs has increased in recent years [2]. Additionally, pharmaceutical companies are increasing the scale of productions resulting in filling vials and syringes in a rapid manner. This increase in the rate of production results in larger equipment being utilized, which leads to increased instability in the proteins [6].

<u>Mass Production of Therapeutic Proteins</u>

In order to bring a therapeutic protein to the market, companies spend years and extensive resources to create and cultivate exact strands of proteins [7]. When making these new proteins, companies begin with small scale equipment to grow and cultivate

the new proteins leading to animal testing, human testing, and eventually FDA approval for human use. In this process, the company is not worried about the quantity of therapeutic protein produced rather the quality of the end product used to gain FDA approval. Once a drug is approved for use in humans and available on the market, companies increase production where the goal is to produce more drugs more efficiently. To do this, the pharmaceutical solution is pumped at higher speeds and pressures to increase the efficiency of the manufacturing process. Additionally, the piping, pumping, and associated valve equipment used to transport the solution is altered because of the new specifications for larger sizes, higher flow rates, and pressures. The significant of the changes in fluid and flow properties when machinery is changed from small to large scale is not evaluated, therefore the retrofitted system has a high potential to cavitate.

Cavitation

Cavitation is a widely recognized and usually undesired phenomenon where a liquid flash boils to vapor and then collapses. Flash boiling in these cases occurs locally due to hydrodynamic, mechanical, or acoustic forces that lower the local pressure to below the critical vapor pressure. This critical pressure is not well correlated to the vapor pressure of the pure liquid and has some dependence on impurities, intensity, and time scale of the applied force. Because this is a local phenomenon once the external force driving the low pressure is removed; pressure returns rapidly to the bulk value and the vapor bubble rapidly collapses. During the collapse of the vapor bubble to the bulk fluid, high velocities are present and collide at a singularity point creating high pressures and large amounts of localized heat. The subsequent dissociation of water can occur, which

generates free radicals. These are localized phenomenon making the temperature and pressure gradient extremely high at the site of cavitation. Although the primary key to understanding when cavitation occurring is well defined the factors that reduce its onset and likelihood are not widely documented.

Cavitation is an undesired phenomenon in many systems (boat propellers, pumps, and piping systems) because the vapor bubbles change the flow characteristics to be turbulent and unsteady. Both of these effects can cause massive vibrations and noise in machinery leading to large reductions in performance and efficiency [8]. In addition to reduced performance, the high pressures resulting from the bubble collapse can cause surface pitting and erosion to all but the toughest metals. However, it is desired in applications such as nebulizers to produce aerosol droplets for drug delivery systems via inhalation. Although there has been little documentation that directly links cavitation to therapeutic protein denaturing, the violent nature of cavitation leads one to understand a possible connection [5,9].

Locations of Cavitation

Although the factors that reduce the onset of cavitation are not readily understood, areas where cavitation is likely to occur are well known. In piping systems, sharp corners, pipe constrictions, pumps, and valves are locations where cavitation can and does occur. This is due to the large increase in velocity in these locations. By means of Bernoulli's equation, an increase in velocity requires a decrease in pressure. Therefore, in these systems where the localized velocity increases greatly, the pressure decreases creating a higher likelihood of cavitation. In piping system, Figure 1.1, utilizing an incompressible

3

fluid, the mass flow rate must remain constant and is a function of cross sectional area of the flow and fluid velocity. As the cross-section of the fluid decreases, the velocity of the fluid must increase to conserve the mass flow rate. This is magnified when the flow separates and creates pockets of recirculation reducing the cross-sectional area of the fluid forcing the fluid to a higher velocity. Sharp corners are problematic because as a fluid passes around a corner it is likely to separate resulting in recirculation, reduction in cross sectional area, and an increase in velocity, ultimately leading to a decrease in pressure. Pumps are problematic because it has sharp edges and fast moving parts. If these parts move fast enough a vacuum or low pressure region is created on the face of the moving part. Valves are problematic because if it is closed quickly without stopping the pumps forcing the flow, a high pressure wave can form on the upstream side of the valve and a low pressure wave can form on the bottom side of the valve. Additionally, as the valve closes, it acts like a constricting channel and if left partially open is a constricting channel where cavitation is likely to occur, Figure 1.1.
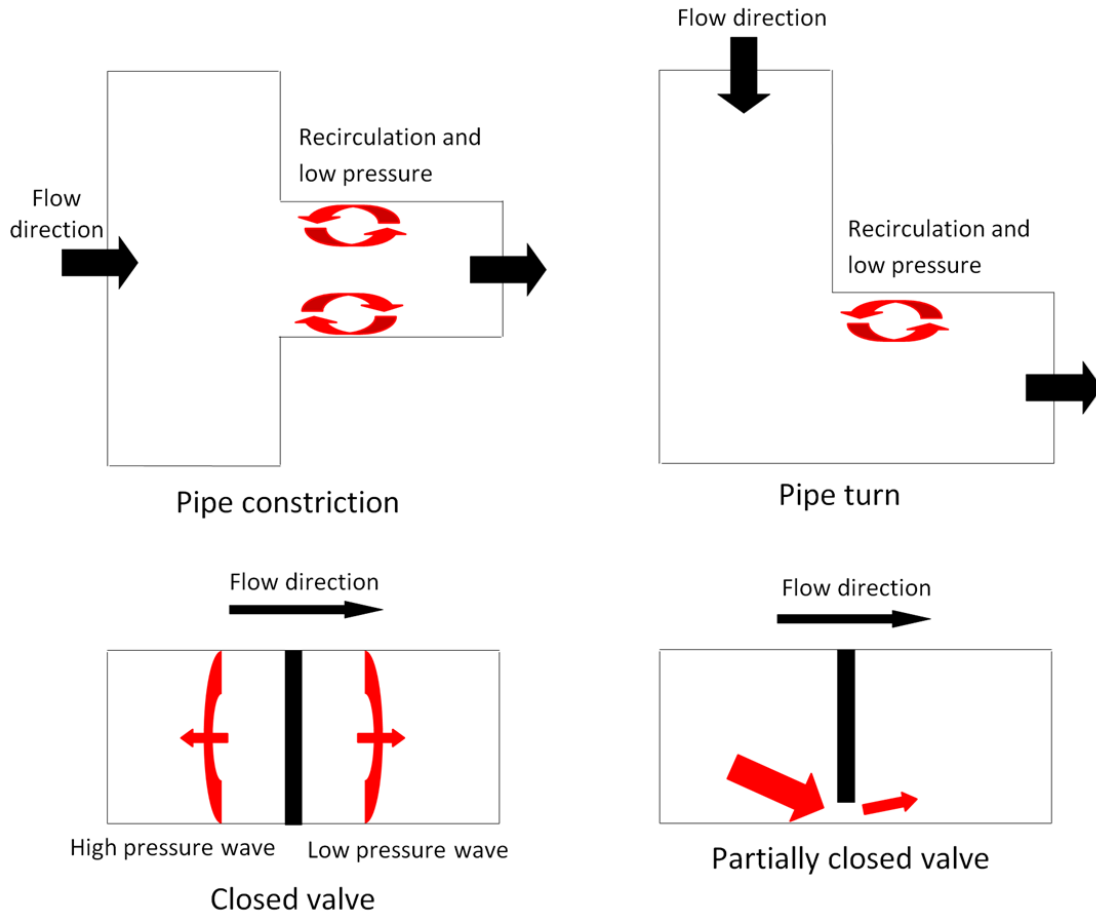
Figure 1.1 – Problem areas where cavitation is likely to occur in pipe constrictions (top left), pipe turns (top right), closed valves (bottom left) and partially closed valves (bottom right).

Cavitation Modeling

Due to the complexity of cavitation and the different ways this phenomenon can occur, modeling cavitation is challenging. Not only does modeling cavitation require a detailed understanding of when a flow cavitates to form a vapor bubble, it also requires understanding when a vapor bubble will collapse back into the bulk fluid. For specific applications custom codes can be created that apply for a specific case, but a generic code that applies across all applications of cavitation is much more challenging. The available codes for specific application include cavitation due to hydrofoils, shock waves,

turbulence, and high speed propellers [9–16]. These models are only valid for their specific application. Singhal et. al. has produced several specific model, similar to the ones previously mentioned, and has produced "the Full Cavitation Model" utilizing a robust algorithm with generic cavitation application [8]. The Full Cavitation Model is currently being utilized by industry and commercially available Computational Fluid Dynamics (CFD) software to model water and oil pumps, inducers, impellers, and fuel injection systems [8]. Although this model is being used in industry with promising results, there are still limitations to this model, mainly in the method of when a bubble collapsing back into the bulk fluid. Research at the University of Denver has utilized the Full Cavitation Model with success. For this research, CFD modeling will be utilized, but without a cavitation model. The goal of this research is to understand the leading factors of cavitation in an attempt to avoid the bubble collapsing back into the bulk fluid. For this reason we are only investigating the flow before cavitation and are not interested in the fluid flow after cavitation has occurred. This will also remove any discrepancies with modeling cavitation and focus on the lead up to cavitation.

Proteins Denaturation

The ionic and covalent bonds holding the molecules in the protein together are very strong, but the secondary bonds holding the shape and structure of the protein are relatively weak compared to ionic and covalent bonds. These secondary bonds can be broken by either chemical or physical instabilities [2]. Physical instabilities include denaturation, aggregation, precipitation, and absorption [2]. When these unique bond structures and shapes of therapeutic protein are broken, the proteins become partially or

fully unfolded. These unfolded proteins can group together to form large aggregates. These larger aggregates are regulated by the FDA and are blamed for the adverse effects seen in patients [3–5]. Recent studies have shown that smaller aggregates, in comparison to previous research, still have the potential to cause adverse effect in patients [17].

Several factors can lead to protein unfolding and aggregation such as amino acid sequence, pH level, temperature, and concentration [17]. Additionally, these proteins have highly hydrophobic and hydrophilic parts. Because of this, when the protein comes in contact with a gas liquid interface, it is pushed and pulled to the point where they can change shape and unfold. In terms of protein stability, cavitation results in at least two events that are undesired. The large temperature gradients and additional gas liquid interfaces produced by cavitation are undesirable because of their potential to cause protein degradation. The focus of this research will be on physical instabilities causing protein degradation.

Past Work

The research involving protein stability was first documented by Hsien We in 1931, but the application of proteins to patients for therapeutic effects is still considered a new treatment [18]. Our previous research has demonstrated and measured the degradation of proteins under shipping and administering conditions.

Cavitation in Ultrasonic Nebulizer

Previous work using an ultrasonic nebulizer to vaporize IVIg proteins demonstrated three important findings: (i) cavitation causes protein degradation, (ii) proteins are the sites for nucleation, and (iii) viscosity plays an important role in the rate

7

of cavitation [5]. Using a Mabis Mist II Handheld Ultrasonic Nebulizer, IVIg proteins were used to evaluate the effects of the gas-liquid interfaces, energy per mass, time effects, and protein concentrations. If the protein is the site of nucleation, the higher the protein concentration in the solution the higher likelihood of cavitation. Although the importance of viscosity was noted in this research, no attempt was made to correlate or explain this phenomenon.

Cavitation in Shipping Collisions

Previous work demonstrated if a therapeutic protein is dropped in the shipping process or by a patient when administering the drug, cavitation occurs [17]. The work demonstrated cavitation occurs and proteins are destroyed when subject to a standard shipping impact. Using a high speed microscope images were taken at a rate of 6000 frames per second of a 3 mL vial filled with 1 mL of 1mg/mL anti-streptavidin dropped using a Lansmont Shock Tower. The vials were dropped from 10, 20, 30 and 40 inches. The shock tower allowed an unobstructed free-fall and controlled collision. In the high speed images, it is clear cavitation occurs due to the visible bubble formed and then the immediate collapse, Figure 1.2.
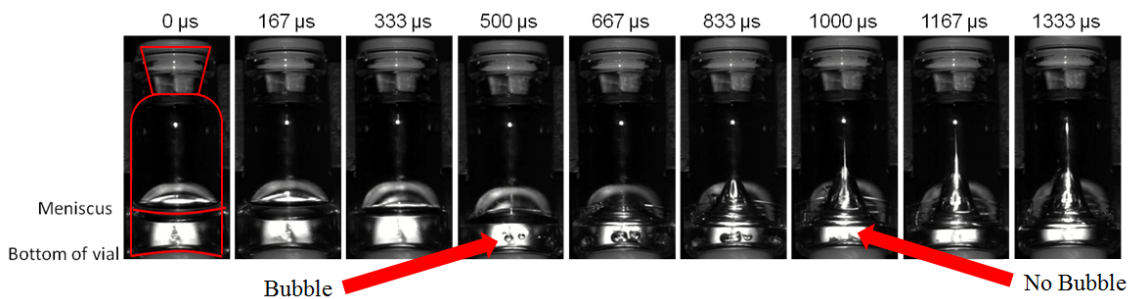
Figure 1.2 – High-speed video frame shots from Lansmont mechanical shock tower.

After the solution was dropped and undergoes an impact, gelatinous particles adhered to the sides of the vials. A BradFord assay was used to quantify the amount of adhered protein. The height of the free-fall is positivily correlated with the amount of protein aggregation, Figure 1.3. This research showed that when a vial of therapeutic proteins undergo an impact it cavitates, aggregates, make it no longer in a usable state for therapeutic benefit. Additionally, the oxidation occurred because free radicals were formed in the solution and free radicals are a direct result of cavitation.
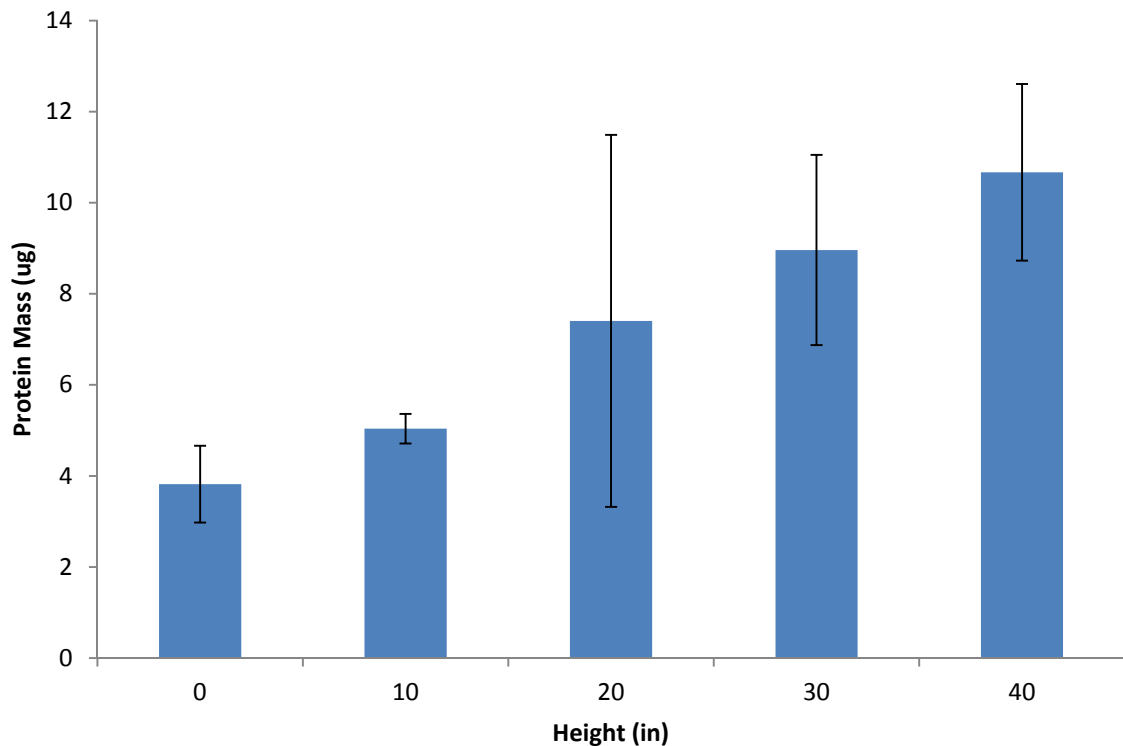
Figure 1.3 – Amount of anti-streptavidin mAb adhering on vial walls of samples after application of mechanical shock in the Lansmont 15D mechanical shock tower as a function of drop height. The mass of adherent mAb was measured by the Bradford assay [17].

The present project is a continuation of previous effort in order to assess the relative risk in terms of the probability for cavitation to be present in a broader variety of pharmaceutically relevant processing and delivery steps. Three specific objectives of the work are to: (i) assess the likelihood of cavitation in other more common processing equipment in terms of non-dimensional fluid parameters, (ii) determine why viscosity appears to dominate cavitating system mitigation, and (ii) explore mitigation strategies for the most violent of cavitating scenarios – that of a vial drop. CFD modeling will be utilized to evaluate the influence of fluid, flow, and geometric parameters on the onset of cavitation. Classical non-dimensional fluid numbers will be evaluated and plotted to characterize the flow patterns in order to understand when cavitation is likely to occur, which should shed light on the dominance of viscosity in mitigating cavitation. The high energy case of vial impact examined via fluid-solid interaction modeling to develop energy dissipation methods that are both cost effective and easy to implement. Finally, the conclusions made through this research will be applied in a more generic way to the manufacturing and delivery devices as recommendations for mitigation strategies.

Outline

This Thesis will characterize hydrodynamic cavitation and mechanical shock cavitation by means of CFD and Fluid Solid Interaction modeling and determine mitigation techniques to be implemented by pharmaceutical manufacturing companies. Chapter 2 will examine hydrodynamic cavitation by means of a constricting channel where CFD modeling is used to evaluate the likelihood of cavitation. Chapter 3 will

examine cavitation due to mechanical shock by means of a high energy impact between a vial and a surface. This analysis will utilize CFD modeling to determine the likelihood of cavitation. Chapter 4 will examine cavitation under the same high energy impact, but FSI modeling will be utilized to couple the fluid and solid models together. Chapter 5 will summarize the results, provide recommendations for pharmaceutical manufacturing companies to mitigate cavitation, and outline future work.

Chapter Two: When Does Cavitation Occur?

Background

Conventional pharmaceutical processes use automated machines to fill vials and syringes for self-administering and administering by a trained professional. The manufacturing and filling process is done on a large scale production machinery where the vial or syringe is filled as fast as possible. To accomplish the high speed filling, the solution is pumped at high pressures in small tubing with pipe constrictions and abrupt turns. Valves are opened and closed quickly creating high pressure waves on the upstream side of the valves and a low pressure wave on the bottom side of the valves. All of these processes add energy to the fluid which can potentially lead to cavitation. As previously discussed, cavitation destroys the native state of the therapeutic protein dissolved in the aqueous solution and has the potential to render the protein unsafe for human administration.

The objective of this research is to assess the risk of cavitation in pharmaceutically relevant conditions and identify some risk mitigation techniques. To accomplish this, Computation Fluid Dynamics (CFD) modeling will be used to model the flow of an aqueous solution over a vast number of operating conditions. The simulation results will be analyzed to identify processes with a high likelihood of cavitating events and propose simple solutions based on driving parameters.

Cavitation is the local phase transformation of a liquid to a vapor phase due to a local low pressure region. In flow induced cavitation, also known as hydrodynamic cavitation, fluid, flow, and geometric parameters influence low pressure regions. For example, Bernoulli's equation, Equation 1, demonstrates that pressure strongly links to local velocity, while the conservation of mass expresses the strong influence of the inlet to outlet area (e.g., diameter ratio for pipes) on local velocity. The influence of constriction edge type on flow behavior as seen through alteration of the minor head loss is less intuitive, Table 2.1. Large values for the head loss term can impose two separate influences on the flow. First, large head losses scavenge flow energy or pressure drop from accelerating velocity. Second, the method by which the energy scavenging occurs is through high turbulence where the energy is used for rotational velocity rather than axial velocity. In systems that comprise areas of high turbulence, the related shear stress is extremely high. When modeling cavitation in these high turbulent areas, the traditional transition point at vapor pressure does not accurately describe when a flow vaporizes and condenses. The critical pressure of the fluid does accurately describe the point of phase changes between liquid and vapor for a turbulent flow [19]. The critical pressure is a function of the strain-rate and the turbulent energy, Equation 5.

$$\text{constant} = \frac{1}{2}v^2 + \frac{p}{\rho} + gz$$

(1)

Classically, the relative importance of geometry, fluid properties, and flow conditions on hydrodynamic phenomena is not conducted via dimensional quantities.

13

Instead non-dimensional terms are created to enable the transfer of the information to a broad range of applications as desired in this case.

Table 2.1 – Minor loss coefficient with different entrance types [20,21].

Entrance Type	Geometric Representation	Minor Loss Coefficient, K
Reentrant		0.78
Square-edge		0.5
Rounded		
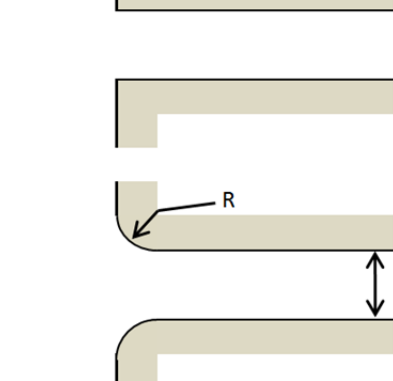
R/D	0.02	0.06	≥ 0.15
K	0.28	0.15	0.04

<u>Dimensionless Numbers</u>

Diameter Ratio

Diameter ratio can be used to characterize the geometric configuration of a contracting or expanding flow. It is typically defined as a ratio of minor diameter to major diameter, Equation 2, where D_r is the diameter ratio, D_{minor} is the minor diameter at outlet, and D_{major} is the major diameter at the inlet.

$$D_r = \frac{D_{minor}}{D_{major}}$$

(2)

14

Reynolds Number

The Reynolds number is the most readily used non-dimensional number in fluid dynamics. It provides the relative ratio of inertial to viscous effects. Although frequently used to monitor the transition from laminar to turbulent flow, it also provides a tool for non-dimensionally describing the dynamic or velocity effects. In Equation 3, ρ is the density of the solutions, v is the mean velocity of the fluid, L is the characteristic length, and μ is the dynamic viscosity of the fluid.

$$Re = \frac{\rho v D}{\mu}$$

(3)

Vapor Pressure

A non-dimensional pressure term can be represented by numerous methods, most of which need information about the vapor and critical pressure to the working fluid. The vapor pressure is the pressure at which fluid changes phase from a liquid to a gas. It is computed by the Clausius Clapeyron equation which is a function of the temperature of the fluid, Equation 4 [20].

$$log_{10}(P_{vap}) = A - \frac{B}{T + C - 273.15}$$

(4)

Where P_{vap} is the vapor pressure of the fluid, T is the temperature of the fluid, and A, B, and C are experimentally determined constants provided by Poling et al. [20].

Critical Pressure

The critical pressure is the point when a fluid will cavitate after considering turbulence. Several methods have been proposed to calculate the critical pressure [19].

15

For this application and under these conditions, the most appropriate equation for the critical pressure is derived by Singhal et al., Equation 5, because it used the turbulent kinetic energy to account for turbulence in the model [8]. Where P_c is the critical pressure and k is the turbulent kinetic energy. This results in a critical pressure equal to the vapor pressure when turbulence is not present and an increase in the critical pressure when turbulence is present.

$$P_c = P_{vap} + 0.195\rho k$$

(5)

Cavitation Number

Cavitation number is a dimensionless number used to characterize the likelihood of a fluid to cavitate via a ratio of pressure difference between the local flow pressure and vapor pressure of the fluid in relation to the dynamic pressure of the system. The Cavitation number is independent of both the flow geometry and turbulence energy in the flow, see Equation 6 [21], where Ca is the Cavitation number and P_{local} is the absolute pressure at a point in the fluid.

$$Ca = \frac{P_{local} - P_{vap}}{\frac{1}{2}\rho v^2}$$

(6)

Pressure Recovery Coefficient

As in all pipes there is a pressure drop along the flow direction of the pipe. This is magnified by the addition of a constriction. The pressure recovery coefficient, C_p, quantifies this pressure loss which is determined by Equation 7, normalized by the dynamic pressure [21]. P_{out} is the pressure at the outlet and P_{in} is the pressure of the inlet.

16

$$C_p = \frac{P_{out} - P_{in}}{\frac{1}{2}\rho v^2}$$

(7)

Energy Length Scale

None of the previous non-dimensional quantities explore the significance of the maximum principal stress or turbulence on the potential for a flow to cavitate. As this can lower the critical pressure by 2-fold, its importance should likely not be ignored. Thus, it is important to quantify the Kolmogorov length scale and the energy dissipation rate by developing associated dimensionless parameters.

The Kolmogorov length scale is a length that characterizes the smallest eddies in a flow. Energy is dissipated in a fluid flow through the energy cascade of eddy dissipation. In each eddy, there are two smaller eddies that transfer the energy to a smaller and smaller length scale. The cascade continues until the Kolmogorov length scale is reached which is indicated by no more smaller eddies and at which point the energy is transferred into heat which is dissipated by the fluid. This energy dissipation happens at all scales of fluid flow. The Kolmogorov length scale is determined by the viscous forces over energy dissipation per mass, Equation 8, where η is the Kolmogorov length scale, γ is the kinematic viscosity, and ε is the energy dissipation rate.

$$\eta = \left(\frac{\gamma^3}{\varepsilon}\right)^{1/4}$$

(8)

Energy Dissipation

The energy dissipation of the fluid was determined by the energy placed in the system per unit mass. This was calculated using Equation 9 derived from Munson et al. where ṁ is the mass flow rate, and m is the mass in the system [22].

$$\varepsilon = \frac{(P_{in} - P_{out})\dot{m}}{m}$$

(9)

Viscosity

Finally, the viscosity of pharmaceutical solutions changes exponentially as a function of solution concentration due to chain entanglement [20]. Therefore, viscosity needs to be represented accurately to provide information on how solution concentration can alter hydrodynamic phenomena. Previous research conducted in the BioFluids Laboratory at the University of Denver has measured the viscosity of the protein solution as a function of solution concentration for IVIg protein. Using an exponential relation, the viscosity of the solution can be determined by its protein concentration using Equation 10 [5]. Where C_1 and C_2 are experimental constants and C_{con} is the concentration of the solutions. The range of concentrations for prefilled syringes and vials is large. For this reason, the range of concentration will be defined from 0 to 25 mg/mL to ensure the entire spectrum of real systems is covered.

$$\mu = C_1 e^{C_2 * C_{con}}$$

(10)

Methods

Model Description

To provide a controlled model that represents a range of pharmaceutical manufacturing processes, with the potential to cavitate, a constricting square-edge channel was created, see Figure 2.1. Parameters that should impact the probability of cavitation in a flow are the fluid properties, the flow properties, and the geometric properties which will be altered to span conditions found in syringe injection and rapid vial filling. A pipe constriction is a good representation of a commonly occurring feature where cavitation is likely to occur and this feature is present in piping systems, pumps, and syringes. The fluid, flow, and geometric parameters altered were:

1. Major diameter (i.e., inlet)

2. Minor diameter (i.e., outlet)

3. Mass flow rate

4. Viscosity

5. Constriction edge type

6. Density
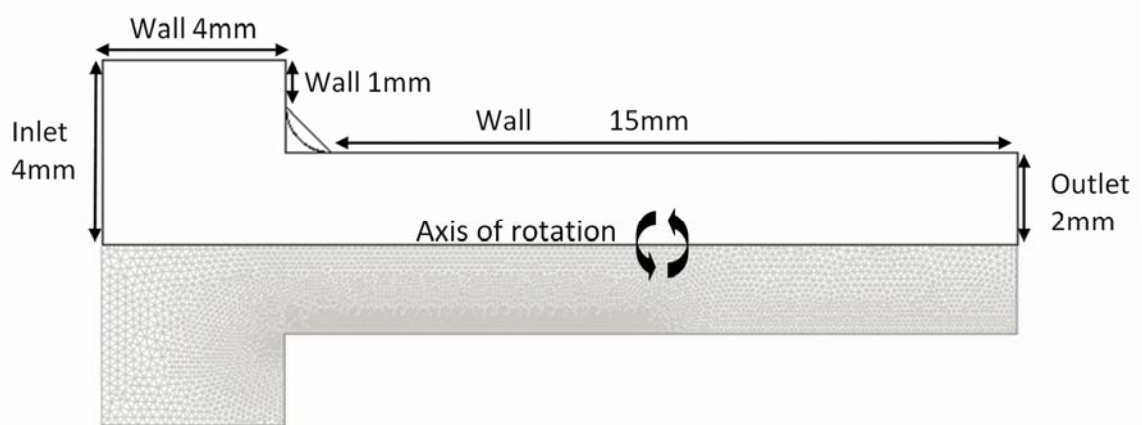
Figure 2.1 – Geometric representation of axisymmetric model with constricting channel with square-edge, 45 degree angle and fillet edge. The inlet height will vary from 2 mm to 40 mm to account for different diameter ratios.

As previously discussed in Chapter 1, cavitation is a function of the localized low pressure which is altered by fluid velocity, turbulence, and principal shear stress. These factors can be affected by fluid properties like viscosity, geometric properties like area constriction, and flow properties like flow rate and inlet turbulence. The diameter ratio will be used to represent changes in the geometric area constriction and the mass flow rate will be used to represent changes in the flow properties. The results from the simulation will be analyzed using non-dimensional numbers to maximize the application of the findings. The computational model proves to be more stable when a mass flow rate is used to control the inlet of the model, rather than a velocity or pressure inlet. For this reason, the density will remain constant, so the mass flow rate is the only factor effecting the flow and velocity of the fluid. The density will be set to a value equivalent to that of an aqueous solution.

Fluid Model

To generate the CFD model ANSYS Fluent™ version 13.0.0 was used. This is a commercially available fluid and thermal software with robust features for turbulence modeling and phase change. To generate the geometric shapes and mesh for each model Gambit® 2.4.6 was used as the preprocessor. Both of these software packages are capable of being run through text commands and are executed through the DOS prompt, allowing the models in each to be manipulated and controlled through a master Matlab code.

The constricting channels were modeled using a 2D axisymmetric algorithm on a HP Z800 Workstation using up to 7 processors. The models ranged in size from 6,000 to 10,000 cells with a max cell skewness of 0.36. The model was run in a steady-state format and implemented with a pressure-based solver because the flow is subsonic and incompressible. This solver utilizes the momentum equation (Equation 11), continuity equation (Equation 12), and the energy equation (Equation 13). Where $\vec{v}$ is the velocity vector, ∇ is the derivative in 3 dimensional space, $\bar{\bar{\tau}}$ is the stress tensor, $\vec{g}$ is gravity, and $\vec{F}$ is external body forces. In the continuity equation S_m is a mass source term. In the energy equation E is the total fluid energy, k_{eff} is the effective thermal conductivity of the fluid, T is the temperature, h is the enthalpy, J is the diffusion flux, $\bar{\bar{\tau}}_{eff}$ is the effective stress tensor and S_h is a volumetric energy source. The standard k-ε turbulence model was implemented with standard wall functions. This turbulence model was implemented because it is specifically for modeling internal pipe flows similar to the case exhibited in

this fluid model [23]. The fluid properties and flow characteristics were altered for each

model and were determined by the master Matlab code.

$$\frac{\partial}{\partial t}(\rho \vec{v}) + \nabla \cdot (\rho \vec{v} \vec{v}) = -\nabla p + \nabla \cdot (\bar{\bar{\tau}}) + \rho \vec{g} + \vec{F} \tag{11}$$

$$\frac{\partial \rho}{\partial t} + \nabla \cdot (\rho \vec{v}) = S_m \tag{12}$$

$$\frac{\partial}{\partial t}(\rho E) + \nabla \big(\vec{v}(\rho E + p) \big) = \nabla \left(k_{eff} \nabla T - \sum_j h_j \vec{J_j} + \big(\bar{\bar{\tau}}_{eff} \cdot \vec{v} \big) \right) + S_h \tag{13}$$

Matlab Code Setup

An evaluation of the entire design space utilized by automated pharmaceutical

filling machines was utilized to determine the overall risk of cavitation. The fluid

properties, flow characteristics, and geometric shape were altered in an systematic

manner so each variable could be analyzed independent of the others. Figure 2.2 is a flow

chart outlining the flow of the Fluent, Gambit, and Matlab codes. The journal files for

Gambit and Fluent were altered by Matlab to encompass the entire design space and the

resulting files were run in the command prompt. The Fluent analysis exported text files

with the desired outputs from the analysis and Matlab read the output variables,

calculated the desired values, and plotted them for analysis. Three different approaches

were used to explore the importance of different variables.
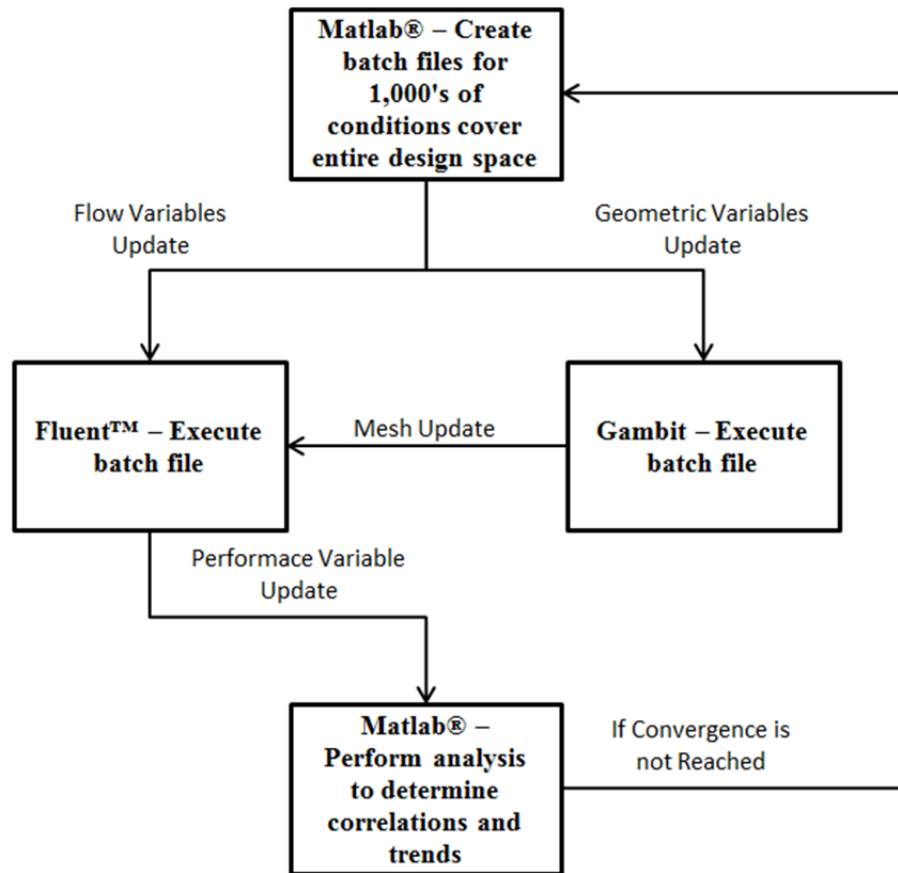
Figure 2.2 – Analysis loop depicting the path by which the software packages pass information to create different models with varying fluid, flow, and geometric properties and then process the results.

Dimensionless Number Methods

The master Matlab code perturbed variables one at a time to create a matrix that consisted of the following parameters in Table 2.2, resulting in 546 models and corresponding data points that were plotted. The minor diameter was held constant and the major diameter was swept from 5.714 to 40 mm to reflect a change in diameter ratio from 0.7 to 0.1. This range was chosen because the 0.7 diameter ratio is representative of a minor pipe constriction and 0.1 is representative of a constriction from a syringe to a

needle. The mass flow rates were altered from 5 to 200 g/s which represents a slow flow

rate to a flow rate used to fill syringes and a fast flow rate used to fill vials [24]. The

viscosity ranged from 5.2 to 97.4 cP which represents a range of fluids from water to a

near gelatin solution. The density was not altered because it was directly related to the

mass flow rate. The inlet was modeled as a mass flow inlet, so altering the density would

directly alter the flow rate into the system. Therefore, changing the flow rate and density

would have the same effect on the system. The turbulence going into the model is

considered negligible with respect to the increase in turbulent energy due to the pipe

constriction.

Table 2.2 – Conditions at which the CFD models were evaluated resulting in 546 models that each produced one data point for the results section.

Major Diameter (mm)	5.7, 6.7, 8.0, 10.0, 13.3, 20, 40
Minor Diameter (mm)	4
Mass Flow Rate (g/s)	5, 8, 10, 20, 30, 40, 50, 60, 80, 100, 130, 160, 200
Viscosity (cP)	5.2, 9.3, 16.8, 30.2, 54.2, 97.4
Density (kg/m^3)	1000

Edge Constriction Type

To determine if the type of edge has any impact the mouth of the constriction was

altered to a 45 degree angled wall and a fillet, Figure 2.1. The same 546 conditions were

replicated for the 45 degree angle and the fillet channel and compared to determine what effect the edge constriction type has on cavitation.

Geometric Scalability of Diameter

In each of the above models the minor diameter was held constant and the major diameter was altered to account for the change in diameter ratio. In this section the diameter ratio will remain constant at 0.5 and the major and minor diameter will be altered to determine what effect they have on cavitation.

Results and Discussion

Dimensionless Numbers

The 546 different cases for the square-edge channel were evaluated resulting in 101 cavitating models. Figure 2.3 shows the diameter ratio as a function of the Reynolds number and grouped into cavitating and non-cavitating conditions. The Reynolds number was calculated at the exit of the minor diameter. Overlaid on the data are regions where vial filling, syringe filling, and syringe discharge operations occur. Syringe and vial filling operations exist in regions where a high number of cavitating cases exist. In the syringe discharge operation there are no cavitating cases that fall directly inside of the bounds of operation, but there are cavitating cases near the bounds. Figure 2.3 demonstrates cavitation occurs in pharmaceutical manufacturing operations and should be addressed when designing new systems. However, Figure 2.3 does little to characterize cavitation because the cavitating cases overlap the non-cavitating, cases indicating a driving mechanism is not identified by the dimensionless quantities.
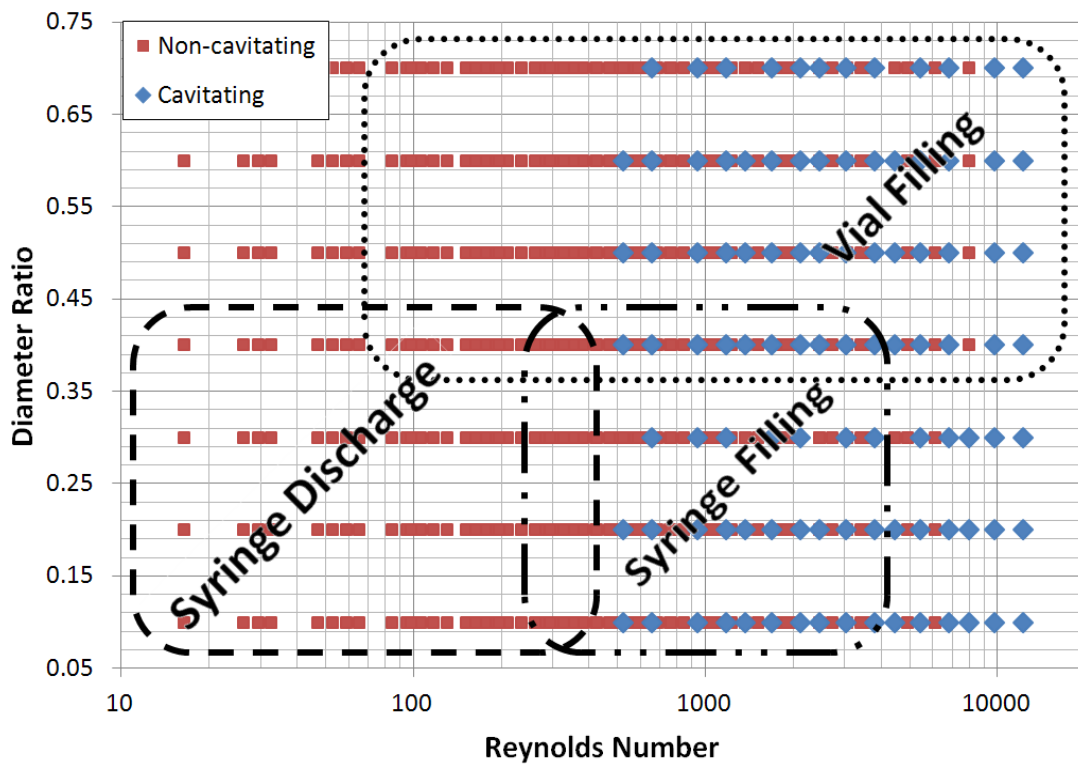
Figure 2.3 – Diameter ratio as a function of the Reynolds Number with the data separated by cavitating and non-cavitating conditions for the square-edge channel. Overlaid on the data are general regions where vial filling, syringe filling, and syringe discharge operations are likely to occur.

Figure 2.4 plots the lowest pressure observed as a function of the Reynolds number with the data separated in cavitating and non-cavitating groups. This figure shows that if the Reynolds number is below 500, cavitation is not likely to occur. However, this figure does not resolve what will happen when the flow is above a Reynolds number of 500 so it cannot be used to quantify when cavitation is likely to occur.

26
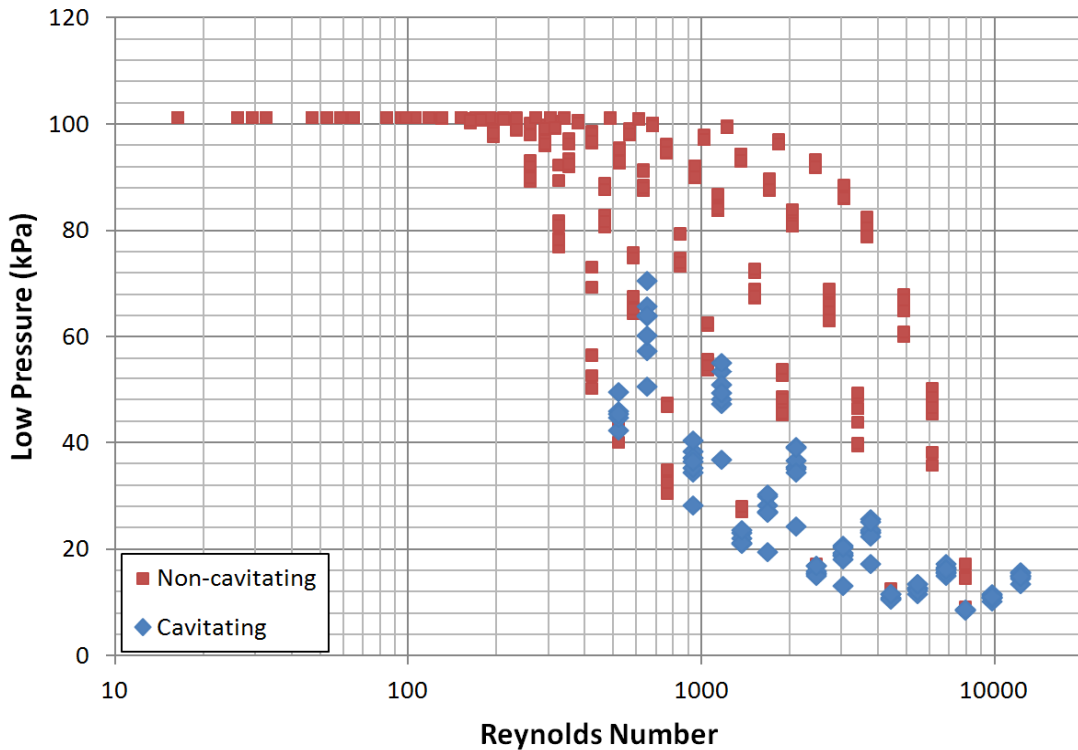
Figure 2.4 – Low pressure versus the Reynolds number for a constricting, square-edge channel using 546 Fluent models with data separated by cavitating and non-cavitating groups.

The Cavitation number is a dimensionless quantity that describes how likely a flow is to cavitate. Figure 2.5 plots the Cavitation number as a function of the Reynolds number with the data separated into cavitating and non-cavitating groups. The velocity term in the Cavitation number is used with respect to the outlet velocity in the minor diameter. This figure shows that if the Cavitation number is below one, cavitation will likely occur. This threshold value is not universal as cavitation is still observed at high Reynolds numbers at Cavitation numbers as low as 0.1. The Cavitation number is calculated using the local low pressure of the fluid. This local low pressure is determined by a myriad of interconnected variables like fluid viscosity, fluid temperature, geometric

27

configuration, turbulence levels, energy dissipation, flow characteristics, principal shear stresses, and operating conditions. This makes the local low pressure a value that cannot be computed by hand. Therefore, it must be experimentally determined or explored through CFD modeling.

Alternatively, the equation for the pressure recovery coefficient, Equation 7, is similar in nature to the Cavitation number, Equation 6, in that they both are a ratio of pressure difference over dynamic pressure. However, the pressure difference in the pressure recovery is determined by the inlet and outlet pressure not the local low pressure. This makes the pressure recovery coefficient much easier to calculate relative to the Cavitation number and this can be done without the aid of experimental measurement or CFD analysis. Figure 2.6 plots the pressure recovery coefficient as a function of the Reynolds number with a contour of diameter ratio. The velocity term in the pressure recovery coefficient is used with respect to the outlet velocity in the minor diameter. Although it is not a collapsed linear line, it does demonstrate that the diameter ratio is reasonably captured by the Reynolds number and pressure recovery coefficient. Therefore, little would be gained from a 3-D plot of the design space. Unlike the Cavitation number, the pressure recovery coefficient, Figure 2.7 does not appear to describe the potential for cavitation in a flow due to the strong overlap at Reynolds numbers above 500.
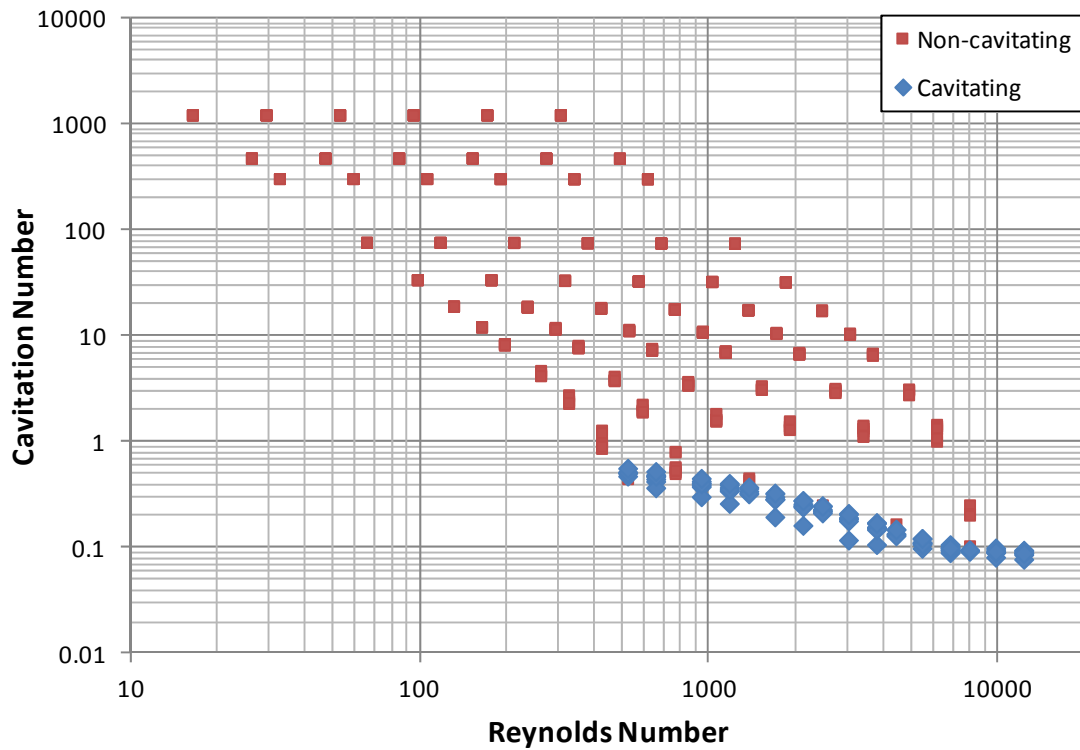
Figure 2.5 – Cavitation number versus the Reynolds number for a constricting, square-edge channel using 546 Fluent models with data separated for cavitating and non-cavitating groups.

29
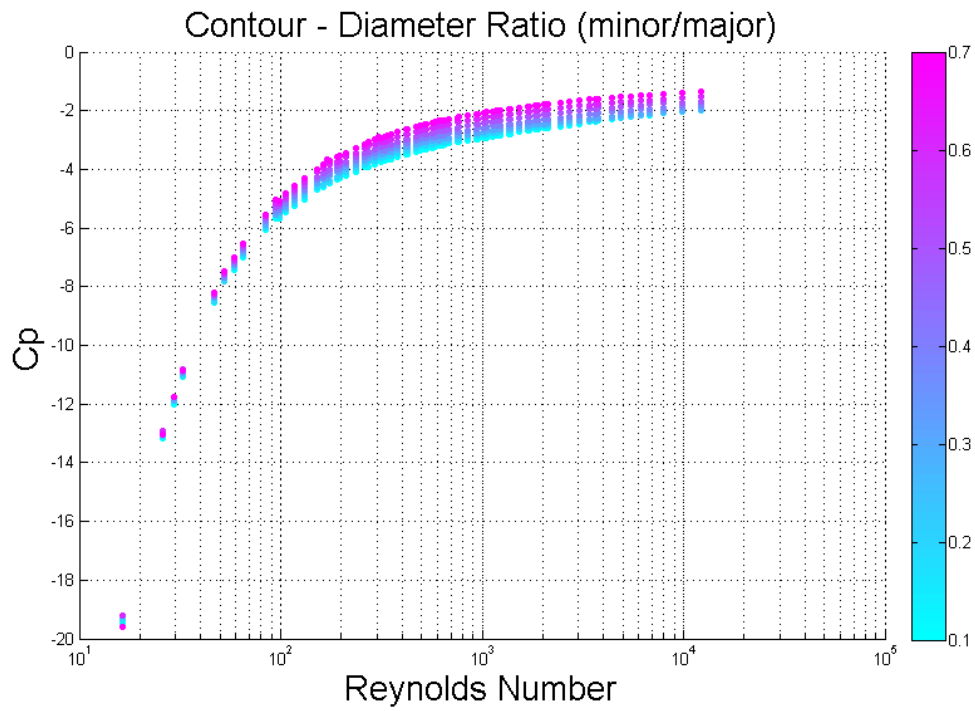
Figure 2.6 – Pressure recovery coefficient versus the Reynolds number for a constricting, square-edge channel using 546 Fluent models with contour colors of diameter ratio.
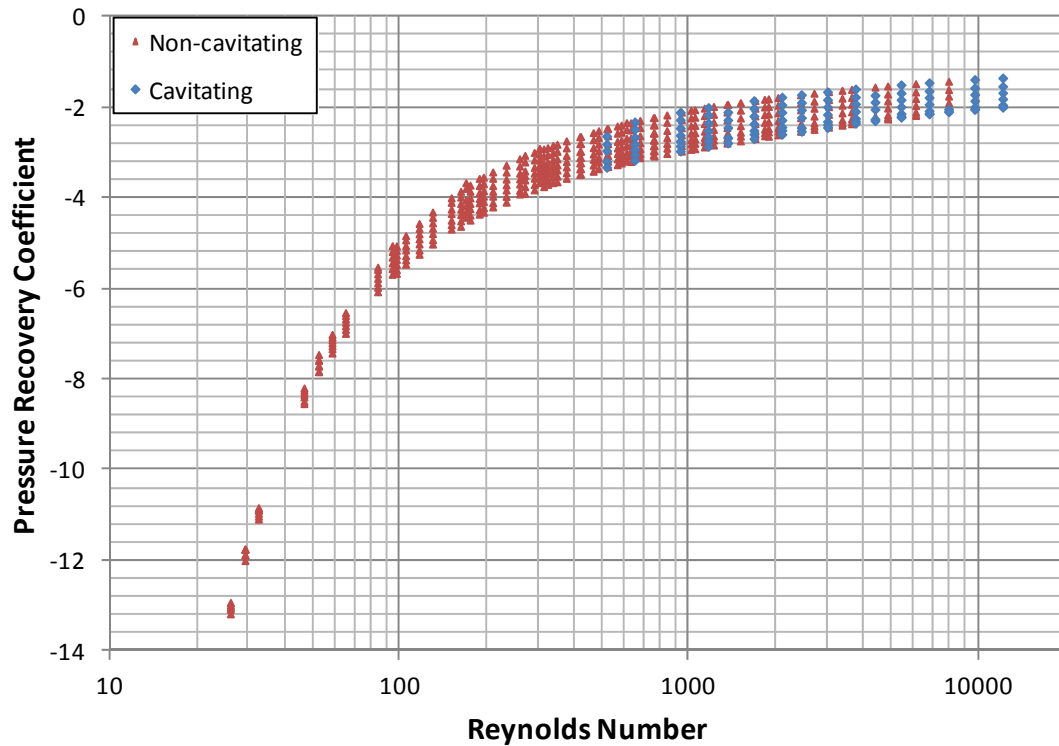
Figure 2.7 – Pressure recovery coefficient versus the Reynolds number for a constricting, square-edge channel using 546 Fluent models with data separated into cavitating and non-cavitating groups.

Edge Constriction Types

To this point, all of the data was for a square-edge constriction type. None of the dimensionless quantities can capture the change in head loss and the resulting turbulence associated with geometric configurations. Due to the nature of the edge types, the square-edge channel has the most turbulent energy and the fillet channel has the least. The same 546 conditions that were evaluated for the square-edge channel were also evaluated for the 45 degree angle and the fillet channels. The mean low pressure increased from the square-edge to the 45 degree angle channel and from the 45 degree channel to the fillet channel. The mean values for the 3 edge constriction types is presented in Table 2.3 and

31

the results from 3 identical conditions with varying edge constriction type are presented

in Figure 2.8. This increase in the mean low pressure is due to the turbulence added to the

system by the type of edge constriction, which also increases the critical pressure. As

more turbulence is added, the critical pressure increases. These changes in critical

pressure and low pressure result in a shift in the likelihood for cavitation. This is very

clear when considering the number of cases that did and did not cavitate. There was a

threefold decrease in the number of cavitating cases from the square-edge to the 45

degree angle, and another significant decrease from the 45 degree angle to the fillet

channel where no cases resulted in cavitation. This clearly demonstrates that changing the

type of constriction to a smoothed edge decreases the likelihood of cavitation.

Table 2.3 – Results from the square-edge, 45 degree angle, and fillet channels under the 546 different conditions.

	Square-edge	Angle channel	Fillet channel
Atmospheric pressure (kPa)	101.3	101.3	101.3
Vapor pressure (kPa)	3.6	3.6	3.6
Mean critical pressure (kPa)	11.0	8.9	5.7
Mean low pressure (kPa)	62.5	88.9	100.8
Cavitating models	101	27	0
Non-Cavitating models	445	519	546
Total models	546	546	546
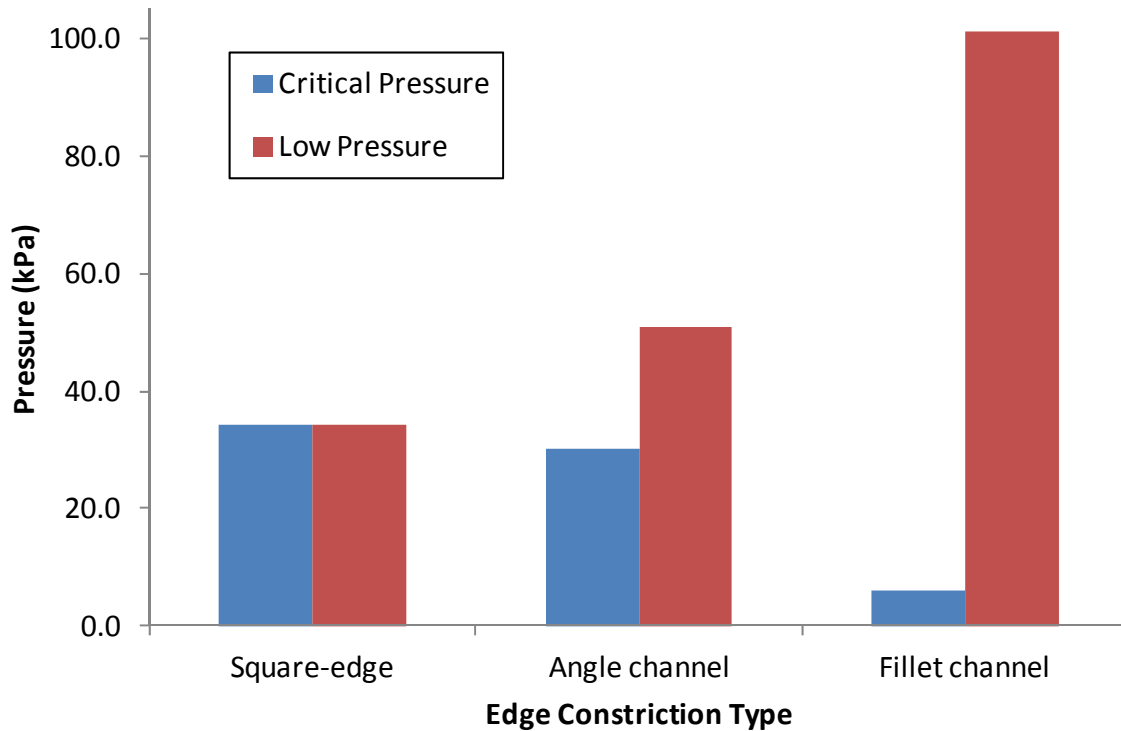
Figure 2.8 – Comparison of critical pressure and low pressure for 3 models under the same conditions except for different edge constriction types.

The effect of turbulence on cavitation can be captured in two methods: (1) modification of the vapor pressure via substitution of the critical pressure or (2) utilization of a non-dimensional flow parameter that captures turbulent strength better than the Reynolds number. The Kolmogorov length scale represents energy dissipation through viscous effects thus providing detailed information on turbulent strength or intensity. Figure 2.9 shows the Kolmogorov length scale as a function of the Reynolds number with a contour of diameter ratio for the three constriction edge types modeled. A linear relationship between the logarithm of the Kolmogorov length scale and logarithm of the Reynolds number indicates that the Reynolds number, diameter ratio, and

turbulence behavior can be captured in the single robust quantity of the Kolmogorov length scale. Returning to plot the Cavitation number as a function of the Kolmogorov length scale, Figure 2.10 demonstrates that regardless of edge constriction type a threshold value for Cavitation can be defined. Figure 2.11 plots the Cavitation number as a function of Kolmogorov length scale with the threshold bounds for separating when cavitation occurs. The threshold for non-cavitating bounds can be found by the following:

Non-cavitating if:

$\eta < 8\ \mu m$ while $Cav > 0.1\eta^{0.8617}$

$\eta > 8\ \mu m$ while $Cav > 0.6$
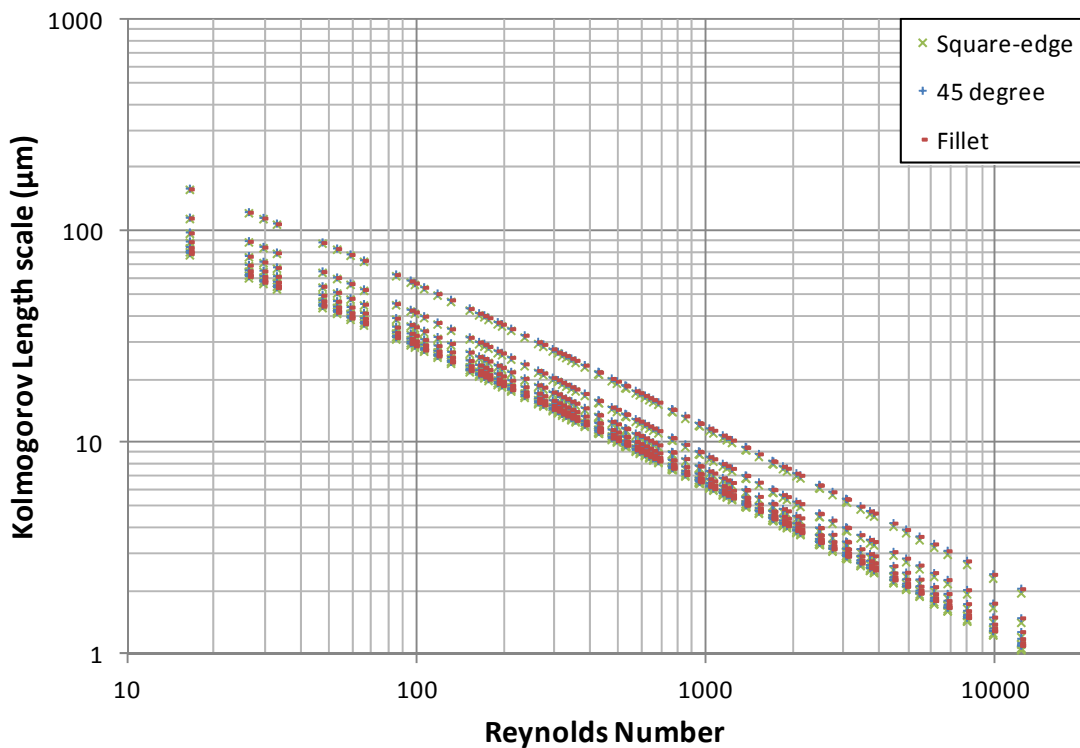
Figure 2.9 – Kolmogorov length scale versus the Reynolds number for constricting square-edge, 45 degree angle, and fillet channels under the same 546 conditions.
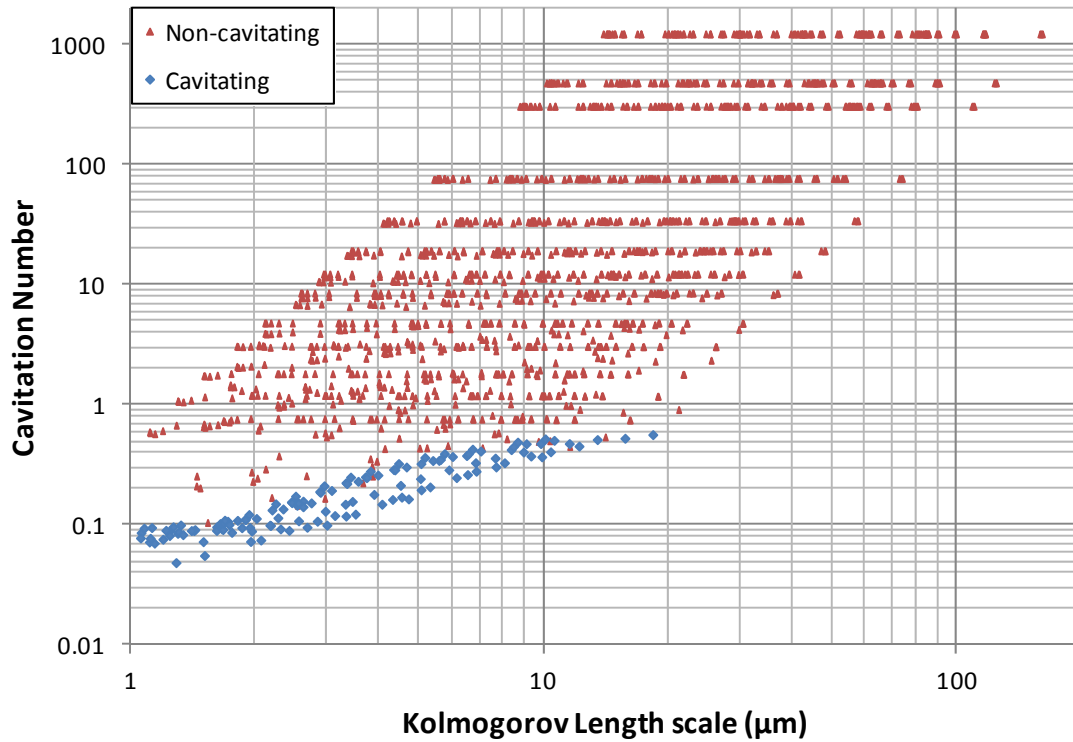
Figure 2.10 – Cavitation number versus Kolmogorov length scale for constricting square-edge, 45 degree angle, and fillet channels under the same 546 conditions with the data grouped into cavitating and non-cavitating cases.
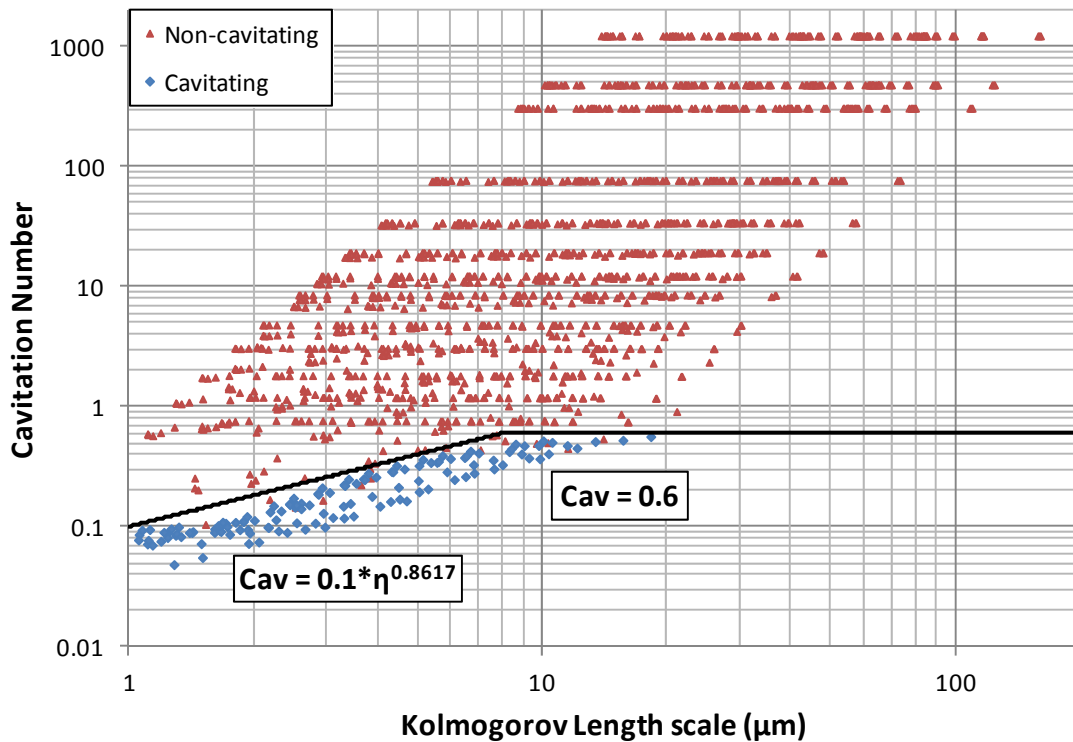
Figure 2.11 – Cavitation number versus Kolmogorov length scale with threshold bounds for dividing cavitating and non-cavitating cases.

Geometric Scalability of Diameter

For each of the previous models the minor diameter was held constant and the major diameter was altered to accommodate the change in diameter ratio. Figure 2.12 shows the Kolmogorov length scale as a function of the Reynolds number for two geometric configurations with the same diameter ratio of 0.5, but different major and minor diameters. The channels have 2 and 4 mm minor diameters and 4 and 8 mm major diameters respectfully. The resulting Kolmogorov length scales for each for the two channels are different, but they both have the same slope. If the Kolmogorov length scale is normalized by the minor diameter, the data collapse onto the same line as shown in

36

Figure 2.13. Returning to plot the Cavitation number as a function of the Kolmogorov

length scale, Figure 2.14 demonstrates that regardless of diameter of the channels, the

threshold value previously defined holds true.
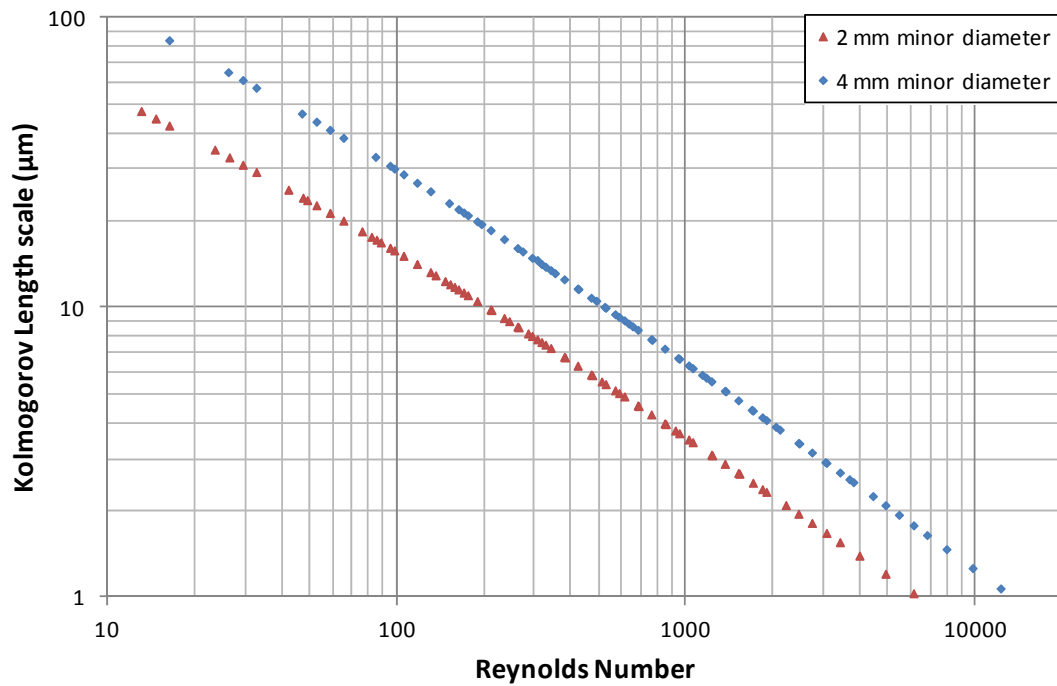
Figure 2.12 – Kolmogorov length scale versus the Reynolds number for two constricting square-edge channels with the same diameter ratios of 0.5, but different minor and major diameters.
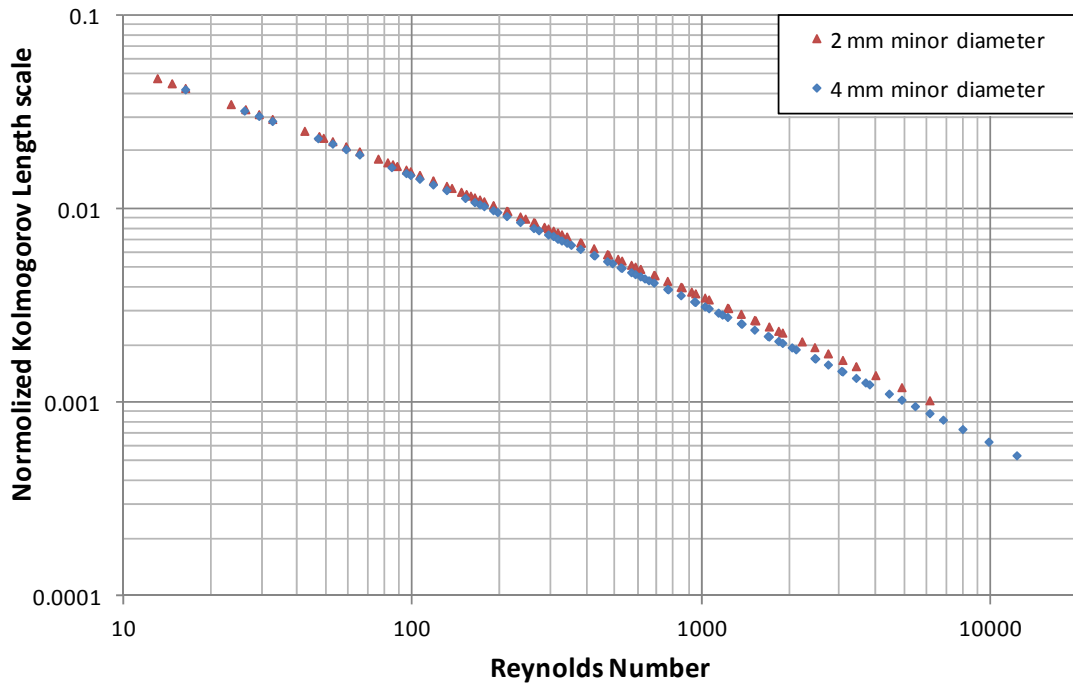
Figure 2.13 – Normalized Kolmogorov length scale versus the Reynolds number for two constricting square-edge channels with the same diameter ratios of 0.5, but different minor and major diameters. The Kolmogorov length scale was normalized by the minor diameter.
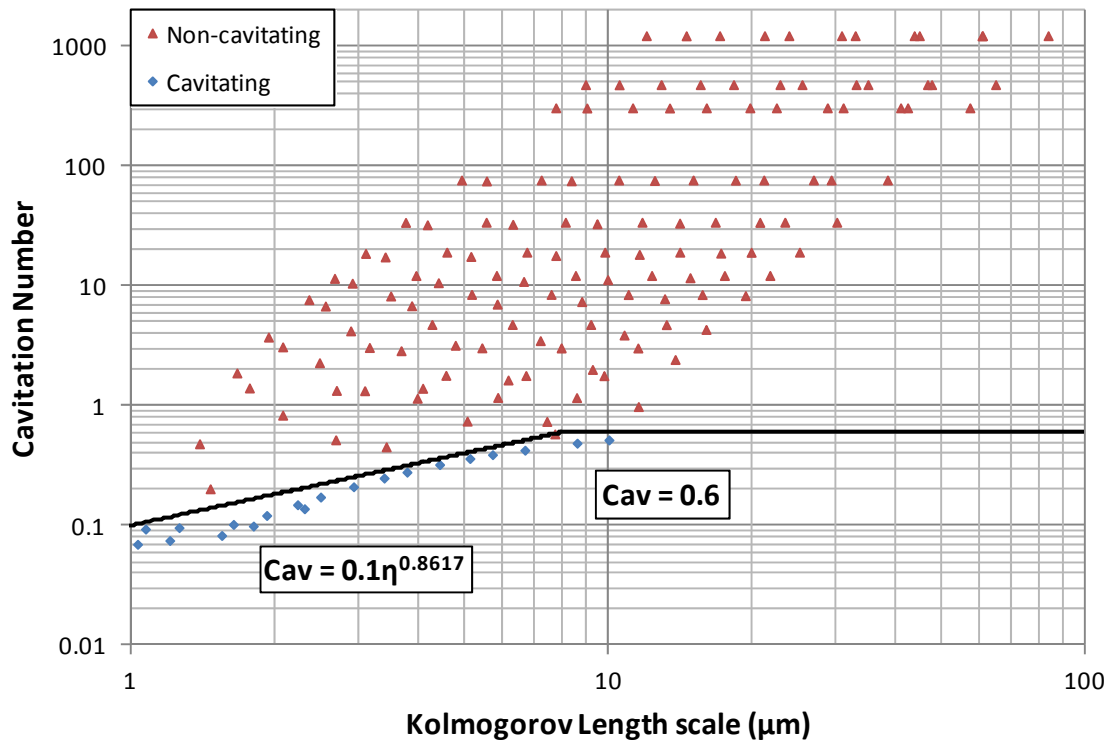
Figure 2.14 – Cavitation number versus Kolmogorov length scale for two constricting square-edge channels with the same diameter ratios of 0.5, but different minor and major diameters. The threshold bounds previously defined are plotted to determine if this trend holds true.

Recommendation for Pharmaceutical Industry

The application of these findings with respect to pharmaceutical manufacturing demonstrates that cavitation is a problem in vial and syringe filling. However, when developing new manufacturing systems steps can be taken to reduce the likelihood of cavitation. The largest impact would be to add a fillet to every edge, but this is not always feasible, so at minimum a tapered edge should utilized. This smoothing of the edge type should be applied in piping systems, pumps, and valves. Next, much more thought should be applied to reducing the amount of turbulence introduced into the system. This can be

39

accomplished by reducing the Reynolds number of the flow. The Reynolds number can

be reduced by reducing the velocity and characteristic length of the system. Third, the

Cavitation number and Kolmogorov length scale should be calculated and applied to the

threshold boundary conditions to determine if the flow is in a cavitating or non-cavitating

region. If these steps are taken when designing new pharmaceutical manufacturing

systems the likelihood of cavitation can be greatly reduced. Proof of this is shown in

Figure 2.15 where a fillet edge is applied to the square-edge channel from Figure 2.3 that

had 101 cavitating cases and under the same conditions the fillet edge had no cavitating

cases.
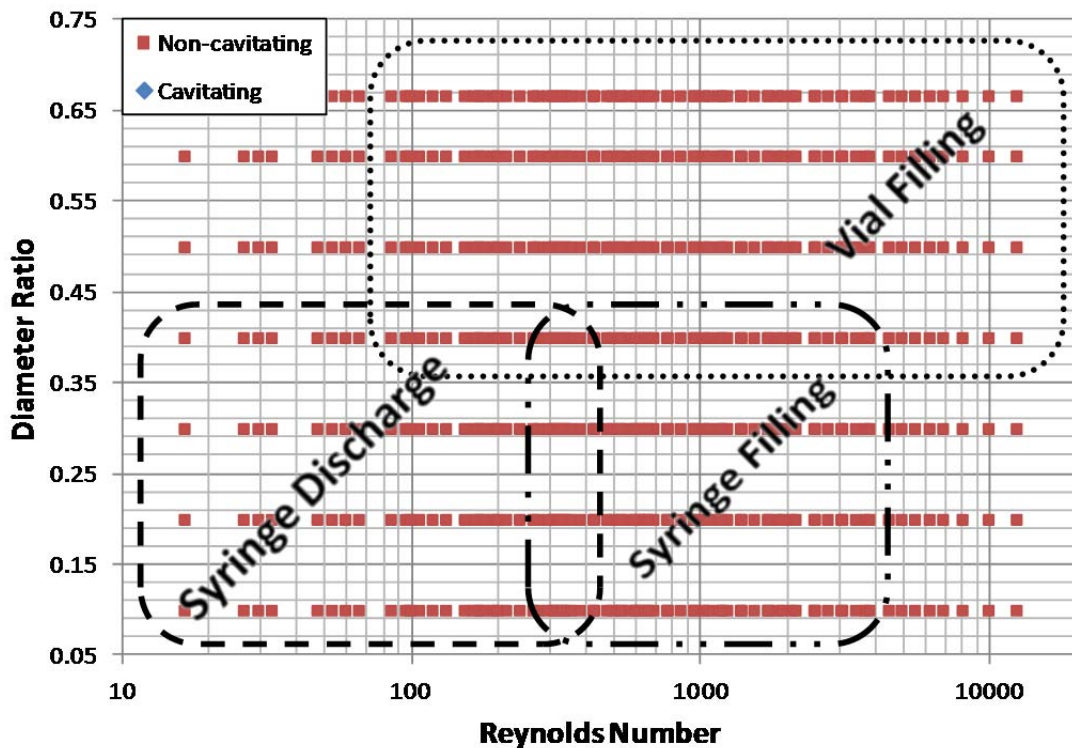
Figure 2.15 – Diameter ratio versus the Reynolds Number with the data separated by cavitating and non-cavitating conditions for the fillet channel. Overlaid on the

data are general regions where vial filling, syringe filling, and syringe discharge operations are likely to fall.

<u>Conclusion</u>

This research shows under current pharmaceutical manufacturing conditions, especially in automated vial and syringe filling operations, cavitation is a real risk that needs to be quantified and mitigated. The most universal method in determining the risk of cavitation is by calculating the Cavitation number and Kolmogorov Length scale and applying them to the threshold. Conservatively, if the Cavitation number is larger than 0.6 or the Kolmogorov Length scale is below 10μm then removing sharp edges by rounding or reducing turbulence by reducing the mass flow rate or increasing the viscosity is recommended. These conditions most likely occur at the outlet of pumps, valves, and reductions of from areas (i.e. fill needles). Chapter 3 will examine if cavitation is an issue in high energy impact cases where the fluid is not flowing continuously though pipes, but instead is subject to a large deceleration rates.

Chapter Three: Fluid Analysis of High Energy Cavitation Cases

<u>Background</u>

After a therapeutic protein is manufactured by medical companies, vials and

syringes are shipped and distributed for patient use. Transporting conditions can include

air travel, ground, and human handling. Each of these methods can impact vibrations and

drop impacts especially if an automated handling system is involved. Even if a package

containing a therapeutic protein is delivered incident free to a patient, the patient can

unpackage the preloaded vial or syringe and accidentally drop it. The research conducted

at the University of Colorado using a mechanical shock tower confirms when a vial of

therapeutic protein solution is involved in a drop scenario, protein degradation and

cavitation occurs [17]. Figure 3.1 shows still frame images, using a high speed camera, of

bubbles in a vial after an impact has occurred.
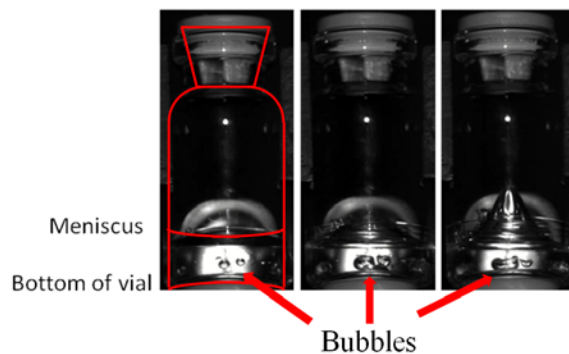
Figure 3.1 – High-speed frame shots of a vial impacting the surface of a mechanical shock tower. Bubbles can clearly be seen which indicates that cavitation has occurred [17]**.**

Energy in Drop

When a vial is dropped and impacts a surface, it experiences high g-forces as a result of the rapid deceleration. These maximum g-forces can be effected by adding packaging material to absorb the impact energy. The energy in the drop comes from the potential energy and is a function of the drop height. The higher the drop height the longer the vial has to accelerate resulting in a higher impact velocity. The rate of deceleration is a function of the vial properties and surface material properties at the point of the collision. For a 30 inch drop height with polyester urethane foam, the g-forces can range greatly from 50 G when 2 inches of foam is used, 130 G when one inch of foam, and higher g-forces when no foam is used [25]. Metal on metal contact is so violent it can produce as much g-force as a pyrotechnic shock [25]. Although the duration of these high g-forces are not long (1μsecond to 1 millisecond), it is known to produce pressure waves that transfer through the vial and into the fluid. These shock or pressure waves emanate from the face of the impact and move at the speed of sound in an outward direction. The pressure waves have a high pressure region at the leading edge and on the back of the wave there is a low pressure region. The question is whether this low pressure wave produces a low enough pressure to cause the fluid to cavitate. The research by the Randolph Group at the University of Colorado demonstrates an impact from a 10 inch drop height causes cavitation and protein degradation [17].

Energy Dissipation Techniques

Adding Packaging Material

Adding energy absorbing packaging material has been used for centuries to transport goods from one point to another. These materials can range from simple paper shavings to complex new foam materials. Therapeutic proteins are typically packaged and sealed in 3 mL vials and placed in energy absorbing material prior to shipping and distribution. When these vials are in packaging material the probability of cavitation is reduced but not immune. For example, Amgen has monitored significant sub-visible particle production in the vials shipped to themselves [17]. Upon removal from the packaging material for storage in a refrigerator or for administering, the probability of a vial drop has not diminished to zero and may be higher especially in cases of Rheumatoid Arthritis patients.

Modeling impact dynamics is challenging because of the time scale over which the shock forms and the velocity it travels (i.e. speed of sound). For that reason experimental testing is typically performed to ensure a package design meets specified standards [25]. If computational modeling is performed, the acceleration curve is usually represented by a half sine wave or a two-term polynomial. Each of these general equations have coefficients that will account for maximum acceleration and duration of the total impacting time [26]. From the acceleration profile a velocity and position profile can be created if boundary conditions are known. Additionally, it is assumed that when modeling an impact the collision is elastic, therefore the object rebounds at the same

velocity it impacted [26]. This is a very conservative assumption because it assumes a higher g-force than actually occurs.

Container Shape

The shape of the container can affect the resulting pressure wave that emanates. For example, if the bottom of the vial is flat a normal shock or pressure wave will form, but if the vial has a curvature the pressure waves could be fanned out and dissipated or focused and amplified. Take the case of a concave vial bottom shape, the pressure waves are focused to the center of the vial and will collide and amplify. However, a convex shape may generate weaker oblique shocks that travel away from the center of the vial. Figure 3.2 shows a visual representation of how wave propagate of a concave and convex surface.
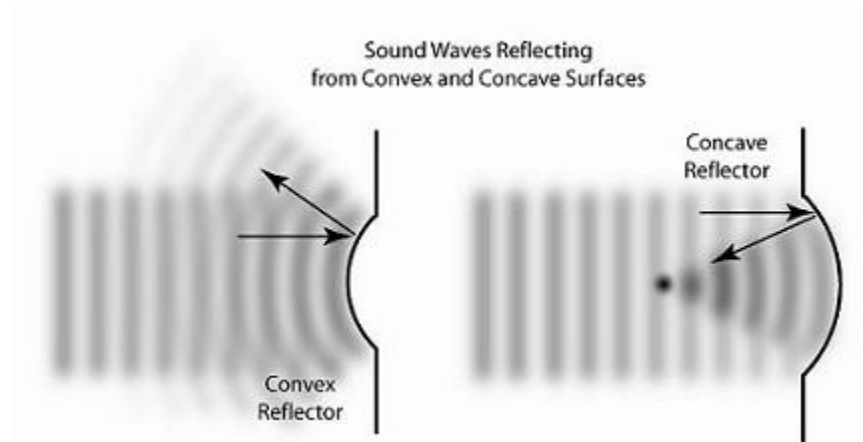
Figure 3.2 – Wave propagation off of concave and convex surfaces [27]**.**

Length Scale Fundamentals

Chapter 2 demonstrated that the Kolmogorov Length scale offers a good indicator for the cavitation potential. The smaller the Kolmogorov Length scale, the more likely

flow is to cavitate. The Kolmogorov Length scale is dominated by energy per mass and the viscosity of the fluid.

Viscous Damping

Viscous fluid damping systems are widely used to dampen vibrating systems and absorb shock. These are found in many applications from mountain bike shocks to fluid built dampers. These systems utilize the viscous effects of fluids by retarding viscous fluid flow through orifices. By changing the viscosity of the fluid in these systems, the rate at which energy is absorbed by the fluid can be tuned.

Energy per Mass

When measuring the intensity of an event such as an impact the energy per mass relation is generally used to relate one event to another. This can be seen when comparing two car crashes with the same mass impacting the same solid object, but at different speeds. The faster moving car will experience more damage because it contains more energy. This energy is absorbed and dissipated through material deformation and buckling. Although both cars have the same mass, they have different energy per mass ratios. The same principles are true for a vial impacting a surface. By altering the energy per mass ratio of the vial, the damage due to impact can be controlled.

Methods

Problem Description

Standard vial shipping containers were explored using 1/3 full, 3 mL vial modeled with varying fluid properties, vial shape, and energy absorbing material properties. Figure

3.3 shows the vial geometry commonly utilized by medical companies. This was the base case used for comparison to altered conditions. The following fluid properties, vial shape, and energy absorbing parameters altered were:

1. Packaging material

2. Contain shape

3. Viscous damping

4. Energy per mass ratio (i.e. density and fill height)

As previously discussed in Chapter 1, cavitation is a function of the localized low pressure which is a function of fluid velocity, turbulence, and principle shear stress. The results from this chapter will be quantified in local low pressure in the fluid system.
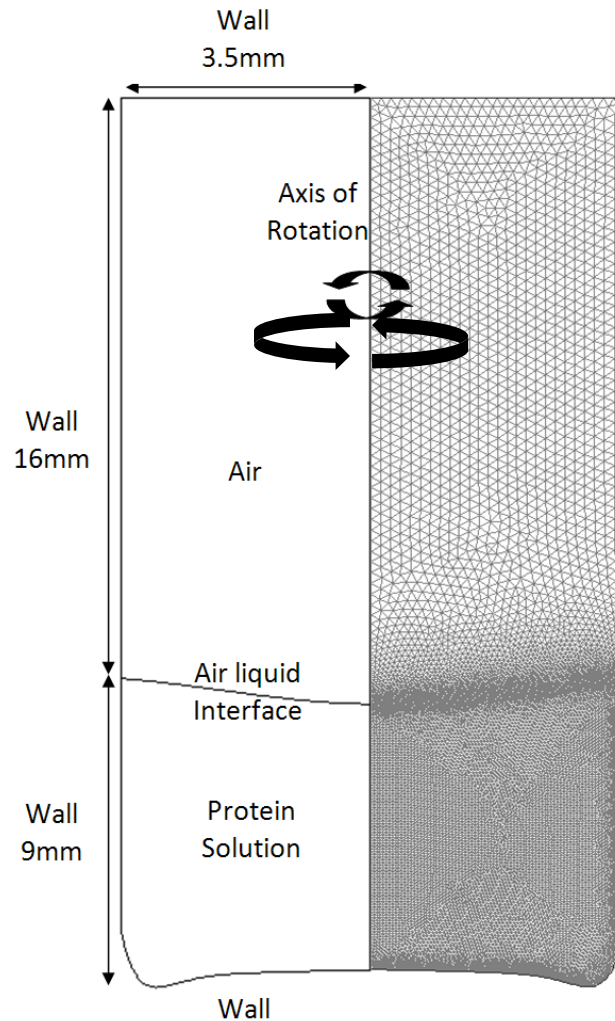
Figure 3.3 – A geometric representation of an axisymmetric vial with an aqueous protein solution. The unique base of the vial is the scanned contour of a standard 3 mL vials.

Fluid Model

To generate the Computational Fluid Dynamics (CFD) model ANSYS Fluent™

version 13.0.0 was again used in conjunction with Gambit® and Matlab. The vial was

modeled using a two dimensionl axisymmetric algorithm on a HP Z800 Workstation

using up to 7 processors. The models contained roughly 20,000 cells with a max

skewness of 0.33. The model was run in a transient format with a time step of 5E-8

seconds and implemented with a pressure-based solver. Traditionally, a density-based

solver is utilized when a flow is supersonic and shockwaves are present, but in this

instance the pressure wave is moving through the fluid at the speed of sound and the fluid

is not at a high Mach number making this model acceptable to run in the pressure-based

solver. An explicit Volume of Fluid (VOF) solving scheme was implemented, which

utilized the momentum equation (Equation 11, Chapter 2), energy equation (Equation 12,

Chapter 2), continuity equation (Equation 14), and volume fraction equation (Equation

15).

$$\frac{1}{\rho_q}\left(\frac{\partial}{\partial t}(\alpha_q \rho_q) + \nabla \cdot (\alpha_q \rho_q \vec{v}_q) = S_{\alpha_q} + \sum_{p=1}^{n}(\dot{m}_{pq} + \dot{m}_{qp})\right) \tag{14}$$

$$\sum_{q=1}^{n} \alpha_q = 1 \tag{15}$$

Where the q represents the number of phases, $\dot{m}_{qp}$ is the mass transfer from phase

q to p and $\dot{m}_{pq}$ is the mass transfer from p to q, α_q is the volume fraction for phase q [23].

The standard k-ε turbulence model was implemented with standard wall functions. A user

defined function (UDF) was added to account for compressible properties not defined in

the standard Fluent database. This included the density of the fluid as a function of

pressure and the speed of sound in the fluid as a function of density. The fluid properties

and flow characteristics were altered for each model and were determined by the master

Matlab code that was used to perturb the variable to explore the design space of pharmaceutical relevance.

Packaging Material

To model different packaging materials, three different acceleration curves were generated to represent a highly padded impact, slightly padded impact, and unpadded impact of a vial striking a solid surface. The initial velocity of the vial at the moment before impact is 4.15 m/s which represents the speed at which a vial would strike the ground if it were dropped from an average height of an individual's hand to the floor. The details of the different conditions are presented in Table 3.1 and the profiles are plotted in Figure 3.4. The duration on the impacts were determined by the amount of time need to return the vial to its original velocity in the opposite direction.

Table 3.1 – Characteristics of 2", 0.5", and no foam padding impacts determined from a two-term polynomial acceleration curve.

Impact description	Initial impact velocity (m/s)	Max g-force (g)	Time duration of impact (ms)
2" Foam pad	4.15	50	25.00
0.5" Foam pad	4.15	500	2.50
Metal on metal impact	4.15	5000*	0.25

*This impact may appear high, but using an accelerometer the Randolph group recorded reading up to the limit of their accelerometer of 1000 G for metal on metal impacts.
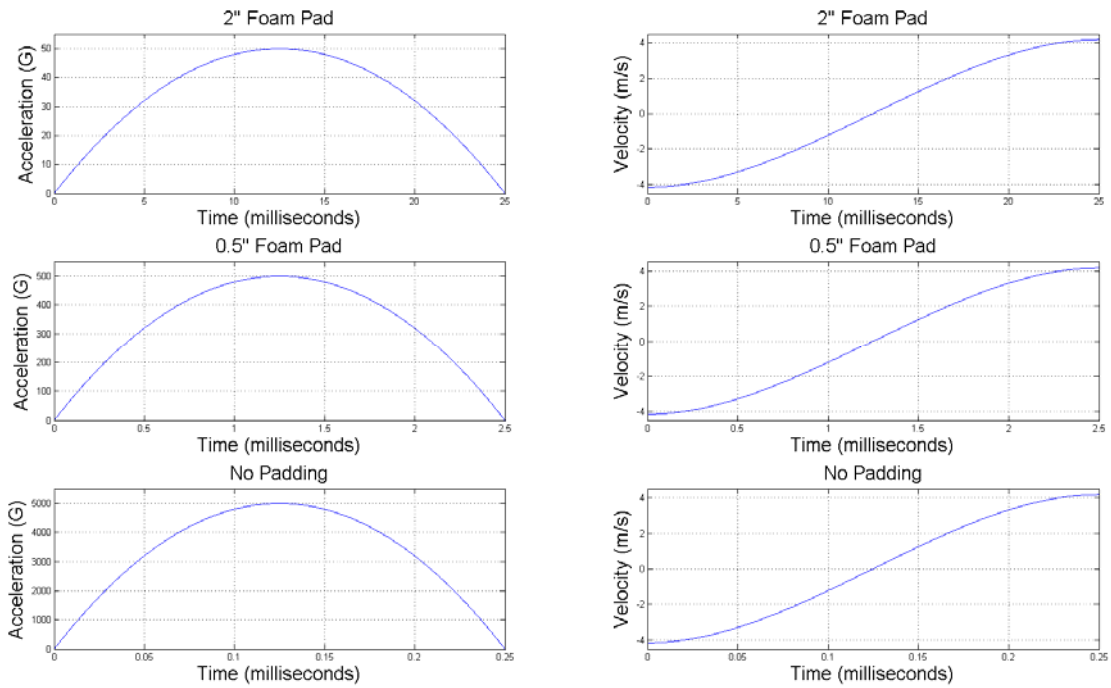
Figure 3.4 – Plot of acceleration and velocity profiles for a 2" foam pad, 0.5" foam pad, and no padding impacts.

Container Shape

To determine the effect of vial shape, specifically the impact surface shape, has on the resulting pressure wave, different vial bottom curvatures were explored. It is not logical to have a concave shape because the resulting pressure wave will propagate back into the fluid. Therefore, a flat bottom and extremely convex shape will be modeled and compared to the standard shape. For this sub-investigation the 500 g-force acceleration impact was utilized because it is in the same range specified in standard package testing [25]. Figure 3.5 shows the geometric representation of the different vial configurations.
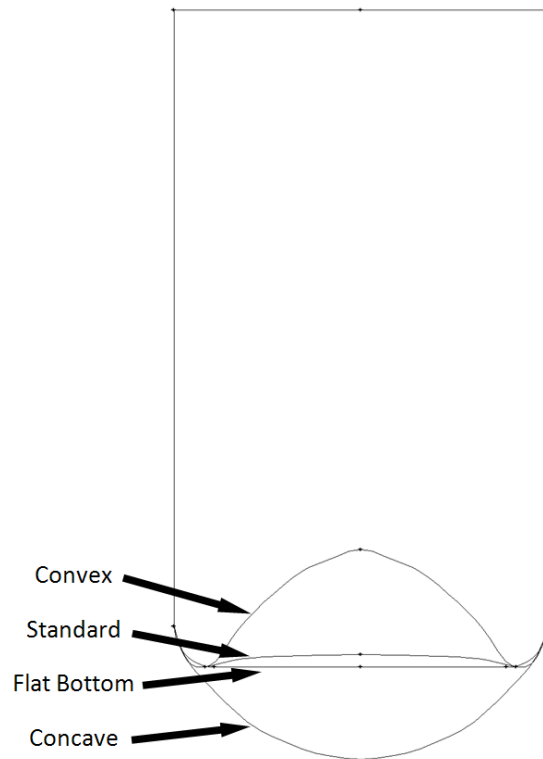
Figure 3.5 – A geometric representation of convex, standard, flat, and concave shapes for the bottom of a 3 mL vial.

Viscous Damping

To determine the effect of the viscous damping in the vial, the viscosity will be altered. Two additional cases were analyzed and compared with the standard 1 cP viscosity of the base model. The two additional cases had a viscosity of 10 and 100 cP which correspond to 10 and 25 mg/mL of IVIg proteins as measured by Giarratano. The 10 cP model represents a fluid with a high viscosity, but still flows easily. The 100 cP viscosity represents a fluid that resembles a gel. For this investigation the slight padded 500 g-force acceleration impact was again utilized to conform to testing standards.

Energy per Mass

To determine the effect of the energy per mass has on the vial impact, two different approaches will be utilized. First, the fill height was changed from the normal 33% full, to 66%, and 100% to add mass to the system. Second, the height of the fluid will remain constant, but the density of the fluid was changed to add mass to the system. The density will be altered from a low protein level of 1000 kg/m^3 to 1200 kg/m^3 and then 1500 kg/m^3.

Results and Discussion

Packaging Material

Adding packing material to absorb impact energy and reduce the deceleration rate can have a positive mitigating effect on cavitation in vials. Figure 3.6 shows the resulting low pressure for each impact case and Table 3.2 reports the exact low pressure values.

Table 3.2 – Low pressure computational results from 2", 0.5", and no foam padding impacts.

	2" Foam Padding	0.5" Foam Padding	No Padding
Low pressure (kPa)	97.0	60.8	0.001

For a vial subjected to an impact with 2" of foam padding, the rebounding fluid resulted in a low pressure cavity of 97.0 kPa, which is not capable of sustaining cavitation, Figure 3.6. For a vial subjected to an impact with 0.5" of foam padding, the rebounding fluid produced a low pressure cavity of 60.8 kPa which is not likely to result in cavitation, based off of results from Chapter 2. For a vial subjected to an impact with

no padding, the rebounding fluid produced a low pressure cavity of 1 Pa, therefore

cavitation will occur.
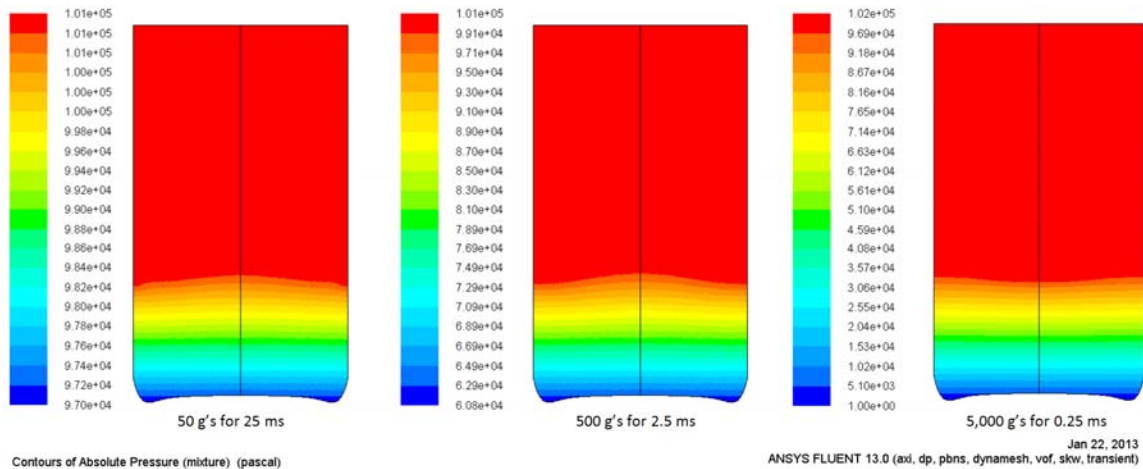
Figure 3.6 – Pressure contour for a 1/3 full vial impacting a surface under 3 different padding conditions. From left to right are the 2" foam pad, 0.5" foam pad and the metal on metal impacts. Cavitation is not likely in the significantly padded impact, possible in the slightly padded impact, and most defiantly in the non-padded impact.

Adding energy absorbing material during shipping therapeutic proteins minimized

the consequence of protein degradation by cavitation in mishandled packages. However,

once a prefilled vial or syringe is out of the packaging and in the hands of a patient, it is

no longer protected and susceptible to being dropped. This is most problematic with the

elderly because they have trouble holding small objects and they have poor sensory and

reflex response. For this reason other energy dissipation strategies must be used in

conjunction with added packaging to eliminate cavitation due to an impact.

Container Shape

The effect of changing the bottom of the vial was examined and the low pressure

in each shaped vial was compared for the 0.5" foam impact. The low pressure did not

change as a function of shape. The low pressure for each of the shapes was 60.8 kPa,

Table 3.3, which is not likely to result in cavitation based off of the results from Chapter

2.

**Table 3.3 – Low pressure results for different bottom vial shapes under the 0.5"
foam padded impact.**

	Standard	Flat Bottom	Convex
Low pressure (kPa)	60.8	60.7	60.8

Viscous Damping

If the viscosity of the fluid is altered there is no difference in low pressure for

either of the 3 impact cases, Table 3.4. There are three potentially reasons the change in

viscosity had no effect on the damping in the fluid system. First, the time scale of

operation is too short to capture the nature of the bulk fluid viscosity. Second, the

rebounding of the vial is not being modeled and therefore, not capturing the effect of the

viscosity changes. Finally, the viscous damping of the fluid is not utilized because the

fluid is not flowing and a mass is not suspended in the fluid.

**Table 3.4 – Low pressure results for different fluid viscosities under the 0.5" foam
impacting conditions.**

	Viscosity (cP)		
	1	10	100
Low pressure (kPa)	60.8	60.8	60.7

Energy per Mass

Fill Height

To change the energy per mass of the system the volume of fluid inside the vial can be altered. Changing this volume had no effect on the likelihood of cavitation until the vial was completely filled with no gas at the top of the vial. Under this condition regardless of the impact condition, cavitation occurred at the top of the vial. Additionally, depending on the case, the fluid is likely to cavitate at a second location near the bottom of the vial as previously seen. The cavitation at the top of the vial is due to the rapid deceleration the vial when the fluid separates from the top of the vial.

Density

A second way to alter the energy per mass ratio is to change the density of the fluid. Altering the density of the fluid results in changes to the low pressure values in the fluid, Table 3.5. As the density increased, the mass in the system is increased, therefore reducing the energy per mass relation and the likelihood of cavitation. The results of the model, however, contradicted this theory showing an increase in the likelihood of cavitation. This can be explained by taking a closer look at the energy per mass equation. The primary source of energy in the vial immediately before impact is kinetic energy so the energy per mass equation becomes Equation 16. When looking at this equation it can be seen that the mass cancels and therefore the equation is independent of the mass. This means the energy per mass is only a function of velocity, which leaves us with the question why is there a difference in the low pressure when mass does not matter. The

answer can be found in the setup of the computational model. The velocity and acceleration curves for the vial are set for all the models regardless of the mass in the system. By examining Newton's Second Law, Equation 17, it is clear that if the acceleration is fixed and the mass changes, the resulting force exerted on the fluid vial system must increase. Therefore, increasing the density of the fluid or the volume in the vial to increase the mass of the overall system will not decrease the likelihood of cavitation if the acceleration and velocity curves for the model remain constant.

Table 3.5 – Low pressure results for different fluid densities under the 0.5" foam impact conditions.

	Density (kg/m^3)		
	1000	1250	1500
Low pressure (kPa)	60.8	50.7	40.7

$$\frac{energy}{mass} = \frac{\frac{1}{2}mv^2}{m} \qquad (16)$$

$$F = ma \qquad (17)$$

Fluid Modeling Limitation

When modeling an impact such as a vial impacting a surface, many assumptions are made to generalize the impact so the fluid model can be solved. In reality, we know that the vial deforms and the resulting acceleration curve is not exactly a two-term polynomial or half sine. By coupling CFD modeling with Finite Element Analysis (FEA) a Fluid Solid Interaction (FSI) model can be implemented where the CFD and FEA models share information to account for the fluid and solid interaction simultaneously. FSI has the potential to add viscous damping to the system via vial deformation and wave

57

propagation through the vial walls. Additionally, the resulting g-forces from the impact will be solved for by the solid model, so no assumption would need to be made about the max g-force and time duration of the impact. FSI modeling can also account for added mass in the vial through density and fill height because the change in mass would change the nature of the impacting vial. Chapter 4 will explore FSI modeling.

Conclusion

This research shows that by changing the packaging material the maximum g-force experienced by the vial can be reduced. This alone is not sufficient to stop all cavitating cases because the vial is not always in the safety of packaging material. CFD modeling shows that altering the density, viscosity, vial fill volume and vial bottom shape are not sufficient methods for mitigating energy to reduce the likelihood of cavitation. However, these changes may have an effect if FSI modeling is used to couple the fluid and solid interactions. Chapter 4 will again examine if cavitation is an issue in extreme impact cases, but it will utilize FSI modeling rather than just CFD modeling.

Chapter Four: FSI Analysis of High Energy Cavitation Cases

<u>Background</u>

As previously discussed in Chapter 3, after therapeutic protein is manufactured it is shipped and distributed for patient use. In the process of transporting therapeutic proteins to the patient, the proteins can travel by air travel, ground, and human handling. Packages containing these proteins can be dropped and vibrated while traveling via planes and automobile, and impacted violently by the sorting equipment. Even if a package containing a therapeutic protein is delivered incident-free to a patient, the patient can unpackage the protein and accidentally drop it. The finds from the research previously conducted in Chapter 3 and the research conducted at the University of Colorado using a mechanical shock tower confirms that when a vial of therapeutic protein solution is involved in a drop scenario, protein degradation and cavitation occurs [17].

The research conducted in Chapter 3 involved Computation Fluid Dynamics (CFD) modeling of a vial impacting a rigid surface. When modeling this impact the acceleration curve was assumed to be a two-term polynomial with a maximum g-force and duration of impact; It was held constant throughout all of the computational models. In reality, the vial deforms and the resulting acceleration curve is not exactly a two-term polynomial. By coupling CFD modeling with Finite Element Analysis (FEA), a Fluid

Solid Interaction (FSI) model can be implemented where the fluid and solid models pass information between models to account for the interactions between the fluid and solid. When switching to a FSI model, the assumptions associated with the impact profile are not made and instead the impact dynamics are solved through the FEA model. This allows the impact dynamics to account for changes in mass and material properties of the vial.

FSI Modeling

The ability to model the coupled relationship between solid material deformation and elastic behavior on fluid flow behavior (and the reverse) is termed FSI modeling. Solid material behavior techniques have largely grown from FEA, whereas the best fluid dynamic simulation methods employ volume of fluid techniques. These are not terribly compatible, and thus require interface information of pressure and geometry remodeling to be transferred between the two algorithms. Therefore, this is a computationally intensive activity, that until recently, was generally considered unfeasible for even fundamental geometries. Published literature on FSI simulations, in fact, has only been around since the late 90's [28]. However, early results were plagued with inaccurate simulation results due to artificial numerical instabilities. Only in the last ten years has the mathematical limitations and ability to apply the technique to more complex geometries become feasible. As a result only a handful of commercially available software can perform FSI modeling, although this is technology is steadily increasing. Common examples that require a fluid solid interaction to generate an accurate solution

60

are the descent of a porous parachute, a piece of cloth falling through air, the flow in a tube constricted with a flexible diaphragm, inflation of a balloon, flow through and around a windsock, and even a patient-specific cerebral aneurysm [28–30].

The current work seeks to utilize FSI simulation in order to (1) accurately replicate the impact dynamics as a function of vial properties, (2) understand the deformation behavior of the vial and its consequences on cavitation within the fluid and (3) explore a few of the variables from Chapter 3 to determine if including the vial properties should be included in therapeutic formulation as implied by the FDA.

Methods

Problem Description

A half full 3 mL vial was modeled with a solid wall at the top of the vial. The fluid geometry is represented in Figure 4.1 and the solid geometry is represented in Figure 4.2. FSI modeling was implemented to capture the vial impacting a fixed surface and the resulting action on the fluid in the vial and the deformation of the vial geometry. The fluid viscosity and vial material properties were changed to explore their effects on the fluid solid system.
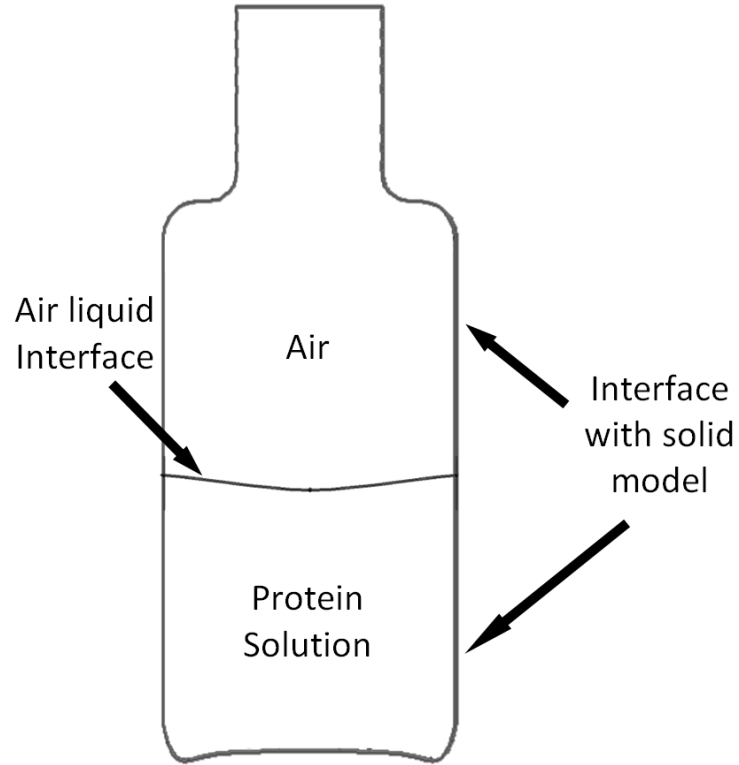
Figure 4.1 – A geometric representation of the cross sectional view of the 3D fluid model.
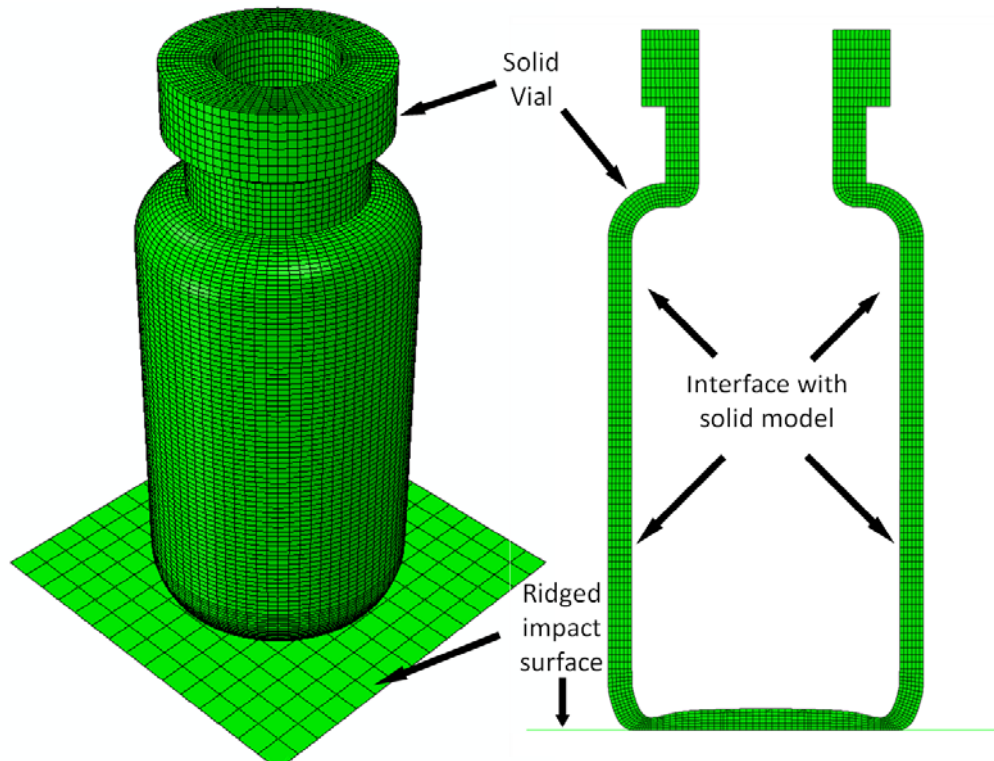
Figure 4.2 – Mesh of solid model evaluated by Abaqus. Left is an isometric view of the entire vial and rigid impact surface. Right is a cross sectional view of the solid vial mesh with the rigid impact surface.

Fluid Model

The CFD model was solved using ANSYS Fluent™ version 13.0.0 in conjunction with Gambit® as the preprocessor. The vial was modeled using a 3D mesh contained roughly 17,500,000 cells with a max skewness of 0.60. The model was run in a transient format with a time step of 5E-8 seconds and implemented with a pressure-based solver. Traditionally, a density-based solver is utilized when a flow is supersonic and shockwaves are present, but in this instance, the pressure wave is moving though the fluid at the speed of sound and the fluid is not at a high Mach number making this model acceptable to run in the pressure-based solver. An explicit Volume of Fluid (VOF)

solving scheme was implemented which utilized the momentum equation (Equation 11, Chapter 2), energy equation (Equation 13, Chapter 2), continuity equation (Equation 14, Chapter 3), and volume fraction equation (Equation 15, Chapter 3). The standard k-ε turbulence model was implemented with standard wall functions. A User Defined Function (UDF) was added to account for compressible properties not defined in the standard Fluent database. This included the density of the fluid as a function of pressure and the speed of sound in the fluid as a function of density. No phase change was specified, so the low pressure in the protein solutions may drop below zero.

Solid Model

The FEA models were solved using Abaqus 6.11 in conjunction with HyperMesh 10.1 as the preprocessor. A mesh was created to represent the vial consisting of approximately 73,000 C3D8 hexaheadral elements with a minimum Jacobian of 0.73. Glass material properties were assigned to the elements of the vial defined in Table 4.1. An element set was created to represent a solid surface for the vial to impact a rigid surface, containing 225 S4R shell elements with a minimum Jacobian of 1. This mesh was fixed in 6 degrees of freedom and defined as a rigid body. General contact between the two mesh surfaces was specified. The loading condition for the vial was an initial downward velocity of 4.165 m/s. A dynamic explicit solving scheme was used to solve the solid model.

64

Fluid Solid Interaction Model

The FSI software used to couple the FEA and CFD models together was MpCCI 4.1.1 (Mesh-based parallel Code Coupling Interface). The computational models were solved on a HP Z800 Workstation with 6 processors dedicated to the CFD Fluent model and one dedicated to the FEA Abaqus model and one for the MpCCI interfacing software. The fluid and solid interface surfaces were linked. The nodal positions for the solid model were used to change the shape of the fluid volume and the pressure in the fluid model was used as an input into the walls of the solid model. The weak coupling algorithm was utilized for interpreting the changes in the nodal values starting with the solid model. Figure 4.3 shows the flow of data through one time step. Because the solid model is initializing the coupled system, the FEA model started the first time step and then passed information to Fluent. If the instability of the FSI model is below one, it is likely to be unstable. The instability is calculated using Equation 18, where ρ_s is the density of the solid, ρ_f is the density of the fluid, h_s is the thickness of the solid, R is the radius of the fluid passageway, and L is the length of the fluid passageway. Under the conditions of this model, the stability of the system was calculated to a minimum of 3.6 [29,32]. Therefore, the model is considered a stable model.

$$\frac{\rho_s h_s \pi^2 R}{\rho_f 2L^2} > 1$$

(18)
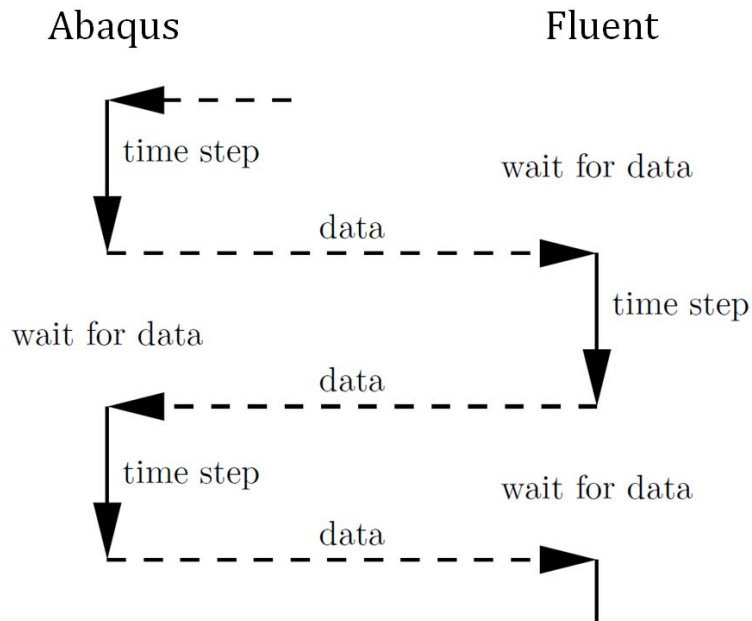
Figure 4.3 – Flow chart depicting the flow of information passed between softwares to complete a time step [31]**.**

Evaluated Models

Three FSI models under different conditions were investigated with the intent of determining (1) how the impact deceleration is altered compared to those assumed in Chapter 3, (2) how the material properties and dynamics of the vial alter cavitation, and (3) if the viscosity still plays an insignificant role in mitigating cavitation under these mechanical shock conditions, in contrast to Chapter 2. All models are run from a similar drop height, fluid density, fill volume and vial bottom curvature. However, the vial material is altered from glass to plastic, and the solution viscosity is raised and compared to a base case. The specific conditions of the three models are outlined in Table 4.1. The high viscosity case will show the potential for changes in the fluid model to alter the

likelihood of cavitation, and the change in the vial material will show potential for

changes in the solid deformation to alter the likelihood of cavitation.

Table 4.1 – Values used by the fluid and solid models for the 3 different conditions evaluated.

		Base conditions	High viscosity	Plastic vial
Fluid Properties	Impact velocity (m/s)	4.165	4.165	4.165
	Viscosity (cP)	1	100	1
Solid Properties	Material name	Glass	Glass	Plastic
	Density (kg/m^3)	2600	2600	1200
	Young's Modulus (Gpa)	70.0	70.0	2.3
	Poisons ratio	0.22	0.22	0.22

Results and Discussion

CFD Modeling and FSI Modeling Comparison

The results from the FSI modeling are different from the results the CFD model

from Chapter 3. The major difference is the assumptions about the impact dynamics. In

the Chapter 3 analysis, the CFD models had a fixed velocity and acceleration curves.

However, in the FSI model the velocity and acceleration curves are a function of the solid

model.

Pressure Wave Propagation

The results of transient coupling of the fluid and solid model resulted in a pressure

wave passing though the fluid at the speed of sound. Images of the propagating wave can

be seen in Figure 4.4 with a pressure wave propagating through the fluid and several low

pressure regions behind the pressure wave. Figure 4.5 shows the shock wave at three

different time intervals. The distance between the waves was measured and the elapsed

67

time between the images results in a wave speed of approximately 1503 m/s. The speed

of sound in a liquid is defined by Equation 19, where c is the speed of sound, E_v is the

isentropic bulk modulus. Comparing the calculated speed of sound, 1497 m/s, with the

measured speed from the images, 1503 m/s, there was less than 0.4% error. The FSI

model was the first model that captured the pressure wave detaching from the vial and

traveled through the fluid. The fact that the wave moves at the speed of sound is a good

check to ensure the fluid system is producing physical results, but it is insufficient to

validate the system.

$$c = \sqrt{\frac{E_v}{\rho}}$$

(19)

Contours of Absolute Pressure (mixture) (atm)

Feb 13, 2013
ANSYS FLUENT 13.0 (3d, dp, pbns, dynamesh, vof, ske, transient)
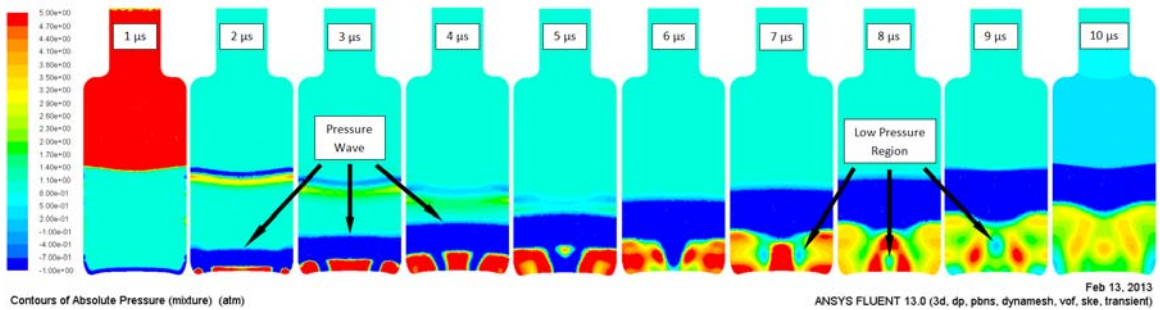
Figure 4.4 – Frame shots of the pressure contour for the transient FSI model. The absolute pressure contour is plotted for a series of images as the model progresses in time. A pressure wave is seen passing through the fluid and several low pressure regions are present behind the propagating wave.

68
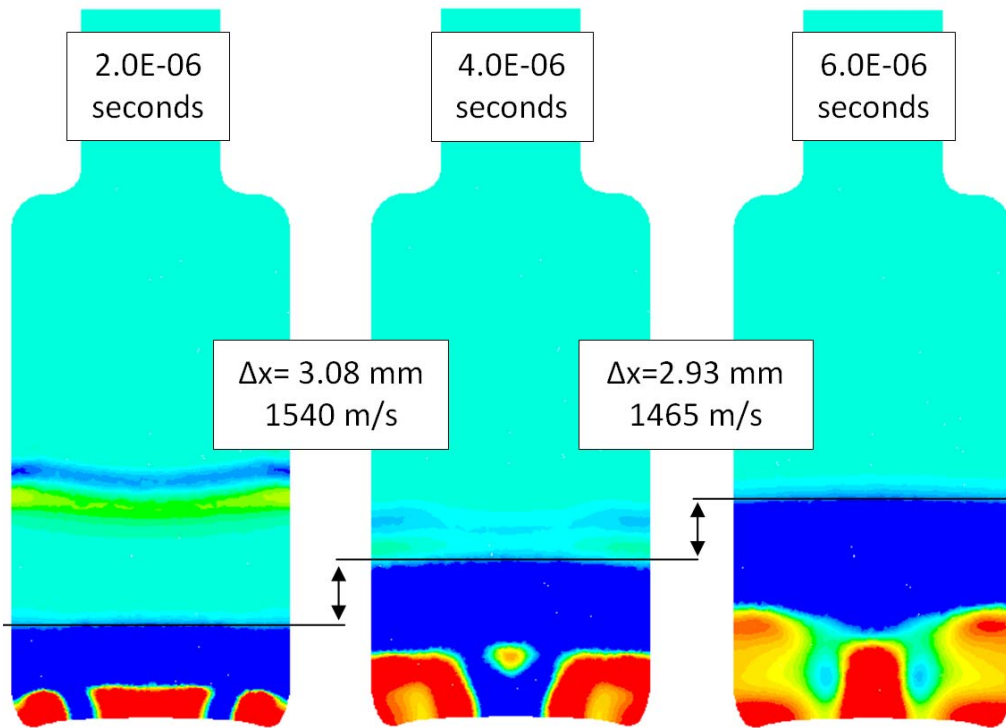
Figure 4.5 – Pressure wave propagating though the liquid solution at the speed of sound. The speed was determined by the distance of the leading edge of the wave and the time difference between images.

Bubble Location

As the low pressure wave passes through the vial and reaches about 10 mm off of

the base (about 4E-6 seconds after impact), the low pressure region remains attached at

the center bottom surface of the vial. Higher pressure regions form in the corner,

indicative a constructive pressure wave reflecting from the side walls. A small pressure

cell is located in the center of vial. This eventually divides the low pressure areas into

two locations, which are similar to the number and locations of the bubbles observed in

experimental images collected by the Randolph Group. Figure 4.6 compares the low

pressure regions in the CFD model and the bubble locations in the images. This is not a

quantitative validation of the model, rather another qualitative identification of

similarities, which were not obtained in the fluid-only simulations of Chapter 3. To

gather quantitative validation, the FSI model would need to include phase change

behavior so that the lifetime of the bubble and diameter could be tracked as a function of

time. The addition of phase change was beyond the scope of the current investigation.
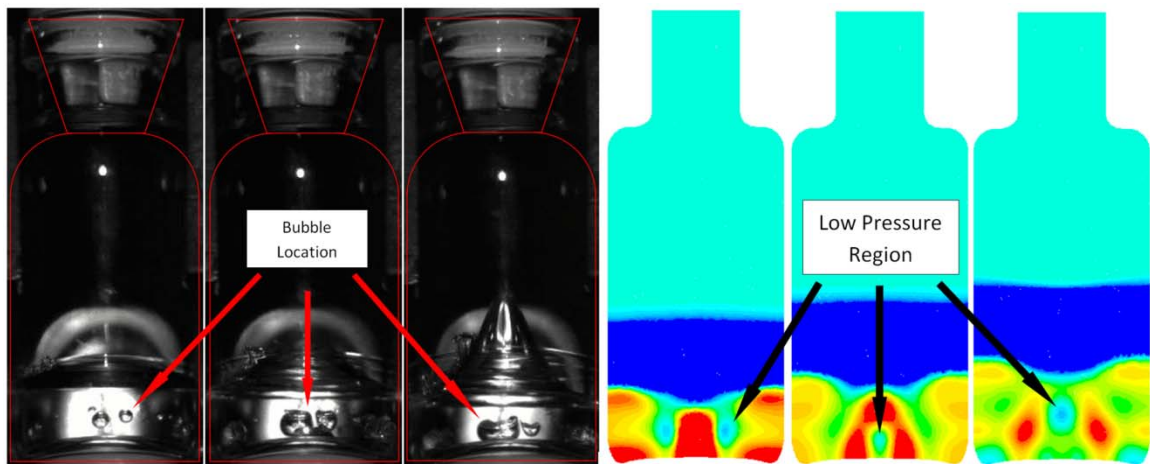
Figure 4.6 – Comparison of the low pressure regions in the CFD model and the bubble locations in the images from the Randolph Group [17]**.**

Viscous Effect

The result of changing the viscosity of the fluid increased the lowest overall

pressure during the simulation, and it suggested that it may have accelerated cavitation.

Figure 4.7 shows the base case compared to the high viscosity case. The lower the

pressure in the wave, the more intensity it carries. When the viscosity is increased from 1

cP to 100 cP, the pressure in the wave decreases, which indicates a stronger pressure

wave passing through the fluid. Due to only analyzing two viscosity conditions, it is

difficult to hypothesize why an increase in viscosity results in a lower pressure and more

intense pressure wave. However, the change in low pressure and pressure wave intensity

does show that changes in the fluid properties can affect the probability of cavitation, in

fact the results of previous research suggest that increasing viscosity can have a

beneficial or harmful effect on cavitation depending on the range [5]. Looking back on

the results from Chapter 3 and the CFD modeling, a change in viscosity had no effect on

the low pressure or likelihood of cavitation. This difference in the results indicates a

deeper study is needed to fully understand the connection between viscosity and

cavitation in an extreme impact case.
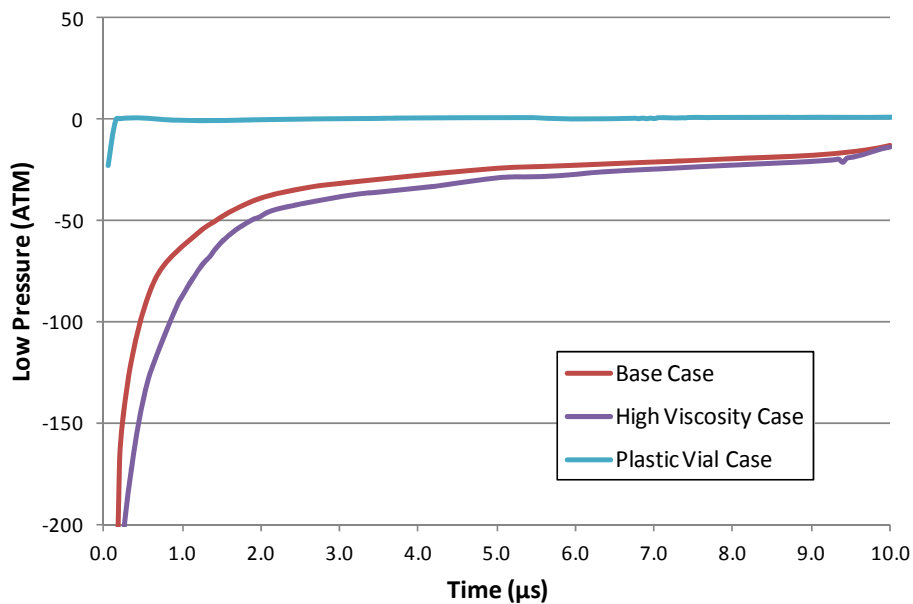
Figure 4.7 – Low pressure versus time in the normal viscosity glass case, high viscosity glass case, and normal viscosity plastic vial cases. No phase change is present, which results in a pressure value of below 0 atmospheres in areas where phase change would occur.

Vial Material Effect

Altering the material properties of the vial resulted in a large increase in the lowest pressure observed indicating cavitation was less strong. The decrease was insufficient to indicate a complete shutdown of the phase change by pressure boiling. Figure 4.7 shows the glass vial case compared to the plastic vial as a function of time. When the material in the vial was changed from glass to plastic, the pressure in the wave increased indicating a weaker pressure wave passing through the fluid. A weaker pressure wave was to be expected because plastic is likely to absorb more energy compared to glass due to its smaller Young's Modulus and ability to deform. This change in the magnitude of the pressure is significant and indicates a deeper study could potentially lead to insightful results.

Conclusion

The result of the FSI models indicate there is a connection between the fluid and solid model and shows that changing the properties in the solid model will change the result in the fluid model and vice versa. Although, this study does produce expected and physical results, a validation of the model should be completed. The FSI modeling also indicates that an impact should not simply be modeled as a two-term polynomial, but rather be a function of the solid model. This work supports the FDA's notion that the vial is part of the formulation of the therapeutic protein system and should be appropriately designed to accommodate the therapeutic protein. This, however, is not the current practice of the BioPharm industry, and thus has the potential for significant impact to

72

industrial practices. Furthermore, additional research is needed to determine the

significance of various fluid properties and vial parameters with respect to the likelihood

of cavitation under high energy impacts.

Chapter Five: Conclusion

<u>Constriction Channel Investigation</u>

A computational fluid dynamics investigation of constricting channels was conducted to assess the risk of cavitation under typical pharmaceutical processing and delivery conditions. An evaluation of the entire automated pharmaceutical filling machine space was evaluated for more than 546 geometric, operating and fluid property conditions. It was determined that cavitation is highly probable in vial and syringe filling operations. The entire data set was utilized to develop a simple method to set a threshold for cavitation that process engineers could utilize to redesign or mitigate cavitating systems. We determined that the Cavitation number and Kolmogorov Length scale provide a robust method to establish this threshold criterion. The threshold for non-cavitating bonds can be found by the following:

Non-cavitating if:

$\eta < 8\ \mu m$ while $Cav > 0.1\eta^{0.8617}$

$\eta > 8\ \mu m$ while $Cav > 0.6$

Based on the results of this investigation, systems that are creating sub-visible protein particles should (1) fillet or round all contraction edges, (2) reduce the amount of energy per unit mass placed into the system or raise the fluid viscosity to increase the Kolmogorov Length scale, and (3) reduce the amount of turbulence in the fluid.

74

To complete this investigation an experimental study should be carried out to verify cavitation is mitigated at the threshold and to demonstrate that this leads to a reduction in the number of sub-visible protein aggregate particles in solution. The threshold validation should include a wide range of constriction flow speeds and constriction edge types to ensure this threshold is universally true.

High Energy Cavitation Cases

A fluid only computational model of a vial drop scenario was simulated to understand if cavitation could be responsible for sub-visible protein particle formation under these conditions. This model utilized a two-term polynomial fit of the acceleration curve without phase change to observe the potential of cavitation after vial impact. Simulations recorded unphysical negative pressure regions on the bottom surface of the vial after impact which indicates phase change would have occurred. These negative pressure regions would be corrected if a phase change model was utilized. An investigation of the solution viscosity, surface curvature, and energy absorbing material revealed that the effect of the viscosity and surface curvature on the low pressure regions were minimal, while the energy absorbing material was sufficient to shutdown cavitation. Studies understanding the influence of fluid density or mass on the behavior of the system indicated limitations and possible failures of the modeling approach.

A Fluid Solid Interaction (FSI) model was developed to couple the fluid and solid system, resulting in a more accurate and robust impact compared to the fixed polynomial. Only a preliminary study was conducted to understand the influence of fluid

and material properties on cavitation. The influence of solution viscosity had only a minor effect; this may be result of the time scale over which the forces and accelerations operate on do not allow sufficient fluid flow reaction time. The influence of vial properties was pronounced, indicating the vial properties (shape and elasticity) could be sufficient to mitigate cavitation in vial drop scenarios. This result argues that the vial should be included in the therapeutic formulation development.

Future work is needed on the computational and experimental side to validate the FSI model by adding phase change so that bubble size, bubble lifetime and interface jetting can be tracked in relation to experimental results. Additionally, an investigation, similar in scope to the one in Chapter 3, should be performed which includes altering fluid properties, material properties of the vial, vial interior and exterior shape, and impact absorbing material between the vial and the rigid surface.

Works Cited

[1] E. Y. Chi, S. Krishnan, T. W. Randolph, and J. F. Carpenter, "Physical Stability of Proteins in Aqueous Solution: Mechanism and Driving Forces in Nonnative Protein Aggregation.," *Pharmaceutical research*, vol. 20, no. 9, pp. 1325–36, Sep. 2003.

[2] M. C. Manning, D. K. Chou, B. M. Murphy, R. W. Payne, and D. S. Katayama, "Stability of Protein Pharmaceuticals: An Update.," *Pharmaceutical research*, vol. 27, no. 4, pp. 544–75, Apr. 2010.

[3] M. Stefani and C. M. Dobson, "Protein aggregation and aggregate toxicity: new insights into protein folding, misfolding diseases and biological evolution.," *Journal of molecular medicine (Berlin, Germany)*, vol. 81, no. 11, pp. 678–99, Nov. 2003.

[4]   a L. Fink, "Protein aggregation: folding aggregates, inclusion bodies and amyloid.," *Folding & design*, vol. 3, no. 1, pp. R9–23, Jan. 1998.

[5] J. Giarratano, "Protein Aggregation Through Acoustic Cavitation," University of Denver, 2012.

[6] M. E. M. Cromwell, E. Hilario, and F. Jacobson, "Protein Aggregation and Bioprocessing.," *The AAPS journal*, vol. 8, no. 3, pp. E572–9, Jan. 2006.

[7] J. a DiMasi, R. W. Hansen, and H. G. Grabowski, "The price of innovation: new estimates of drug development costs.," *Journal of health economics*, vol. 22, no. 2, pp. 151–85, Mar. 2003.

[8] A. K. Singhal, M. M. Athavale, H. Li, and Y. Jiang, "Mathematical Basis and Validation of the Full Cavitation," *Journal of Fluids Engineering*, vol. 124, no. September, pp. 617–624, 2002.

[9] A. Kubota, H. Kato, and H. Yamaguchi, "A new modelling of cavitating flows: a numerical study of unsteady cavitation on a hydrofoil section," *Journal of Fluids Engineering*, vol. 240, pp. 59–96, 1992.

[10] Y. Wang and C. E. Brennen, "SHOCK WAVE DEVELOPMENT IN THE COLLAPSE OF A CLOUD OF BUBBLES," *ASME FED*, vol. 194, no. Cavitation and Multiphase Flow, pp. 15–19, 1994.

[11] A. Keller and H. Rott, "The Effect of Flow Turbulence on Cavitation Inception," *ASME Fluids Engineering Division Summer Meeting*, 1997.

[12] C. Hsiao and L. Pauley, "Numerical Study of Tip Vortex Cavitation Inception Using a Bubble Dynamics Model," *ASME FED Meeting*, 1997.

[13] J. K. Choi and S. A. Kinnas, "Cavitating Propeller Analysis of a Tunnel," *ASME FED*, 1997.

[14]   F. Patella, R. Reboud, and J.-L., "A New Approach to Evaluate the Cavitation Erosion Power," *ASME Journal of Fluids Engineering*, vol. 120, no. 2, pp. 335–344, 1998.

[15]   R. F. Kunz, T. S. Chyczewski, D. R. Stinebring, and H. J. Gibeling, "MULTI-PHASE CFD ANALYSIS OF NATURAL AND VENTILATED CAVITATION ABOUT SUBMERGED BODIES," *ASME Fluids Engineering Conference*, pp. 2–9, 1999.

[16]   R. Avva, A. Singhal, and D. Gibson, "An Enthalpy Based Model of Cavitation," *ASME Paper*, vol. 226, pp. 63–70, 1995.

[17]   T. Randolph and E. Schiltz, "EFFECT OF MECHANICAL SHOCK ON PROTEIN AGGREGATION AND PARTICLE FORMATION," in *Workshop on Protien Aggregation and Immungicity2*, 2012.

[18]   H. Wu, "Studies on the Denaturation of proteins, XIII. A theory of Denaturation," *Chinese J. Physiol.*, vol. 5, pp. 321–344, 1931.

[19]   S. B. Martynov, D. J. Mason, and M. R. Heikal, "Effect of Viscous Stress on Cavitation Flow in Nozzles," *Journal fo Fluids Engineering*, no. 09 August 2006, 2006.

[20]   B. E. Poling, J. M. Prausnitz, and J. P. O'Connell, *The Properties of Gases and Liquids*, 5th ed. New York: , 2000, pp. 7.3–7.7.

[21]   R. W. Fox, A. T. McDonald, and P. J. Pritchard, *Introduction to Fluid Mechanics*, 6th ed. Hoboken: , 2004, pp. 284–286, 336–349.

[22]   C. S. Lengsfeld, L. Munson, Y. K. Lentz, and T. J. Anchordoquy, "DNA Hydrodynamic Degradation Controlled by Kolomogorov Length Scales in Pipe Flow," *Jounal of Pharmaceutical Sciences*, vol. 100, no. 8, pp. 3088–3095, 2011.

[23]   ANSYS, "Fluent Users." [Online]. Available: www.Fluentusers.com.

[24]   Brosch_LLC, "Bosch Products," 2012. [Online]. Available: http://www.boschpackaging.com/Boschpharma-us/eng/64350_63978.asp#. [Accessed: 12-Sep-2012].

[25]   J. F. Hanlon, R. J. Kelsey, and H. E. Forcinio, *Handbook of Package Engineering*, 3rd ed. Lancaster, Pennsylvania: Technomic Publishing Company, 1998, pp. 513–536.

[26]   C. W. De Silva, *Vibration Monitoring, Testing, and Instrumentation*. Boca Raton, FL: CRC Press, 2007.

[27] J. Fuchs, "John's Conrner Technocal Blog," *Upright Communications*, 2011. [Online]. Available: http://www.ctgclean.com/tech-blog/2011/09/ultrasonics-understanding-sound-waves1/. [Accessed: 07-Feb-2013].

[28] J. Jacobs, "TOWARDS A FLUID SOLID INTERACTION MODEL OF A DYNAMIC LUNG," Univeristy of Denver, 2012.

[29] T. E. Tezduyar and S. Sathe, "Modelling of fluid – structure interactions with the space – time finite elements : Solution techniques," *INTERNATIONAL JOURNAL FOR NUMERICAL METHODS IN FLUIDS*, vol. 54, no. 6–8, pp. 855–900, 2007.

[30] T. E. Tezduyar, K. Takizawa, T. Brummer, and P. R. Chen, "Space – time fluid – structure interaction modeling of patient-specific cerebral aneurysms," *INTERNATIONAL JOURNAL FOR NUMERICAL METHODS IN BIOMEDICAL ENGINEERING*, vol. 27, no. 11, pp. 1665–1710, 2011.

[31] Fraunhofer, "MpCCI Documentation." .